The structural behaviour of hybrid steel-trussed concrete beams: A literature review of experimental tests and theoretical models

Structures 71 (2025) 108018

Contents lists available at ScienceDirect

Structures

journal homepage: www.elsevier.com/locate/structures

The structural behaviour of hybrid steel-trussed concrete beams: A literature review of experimental tests and theoretical models

Alessia Monaco [a,*], Piero Colajanni [b], Lidia La Mendola [b]

[a] Politecnico di Torino, Department of Architecture and Design, Viale Mattioli 39, Torino, 10125, Italy
[b] University of Palermo, Department of Engineering, viale delle Scienze, Edificio 8, Palermo, 90128, Italy

ARTICLE INFO

Keywords:
Hybrid steel-trussed concrete beams
Experimental tests
Theoretical models
Stress transfer mechanisms
Flexural behaviour
Shear behaviour
Beam–column joints
Long-term behaviour
Size effect

ABSTRACT

Hybrid Steel-Trussed Concrete Beams (HSTCBs), introduced in civil construction around the 70s, combine a steel truss within an in-situ cast concrete core, often with a steel or concrete bottom plate. Initially favoured in industrial buildings for their semi-prefabricated construction and ability to span large distances with contained depths, HSTCBs have subsequently attracted scientific interest in residential construction, focusing on static and seismic response. The technical literature on this topic highlights that HSTCBs do not follow the same mechanical rules of RC or steel-concrete composite beams, necessitating specific insights into their behaviour under flexure, shear, and seismic conditions. This review aims to collect the major scientific results obtained in the last twenty-five years by several researchers in Italy and abroad, beside the outcomes of some relevant earlier studies. The reviewed papers encompass findings from experimental campaigns on weldings, push-out test specimens, simply supported beams and beam-to-column joints. Some of these studies also incorporate proposals for analytical formulations aimed at offering design-oriented and code-compliant prediction models, alongside finite element simulations to replicate the strengthening mechanisms. Following a thorough synthesis of the primary findings to date, the literature review underscores notable gaps in knowledge and still open issues, particularly concerning long-term performance and size-effect laws.

1. Introduction

The structural performance of Hybrid Steel-Trussed Concrete Beams (HSTCBs) has been studied since the ’70s by the scientific community, and their adoption in civil construction has been widened since the 2000s. These beams are constituted by a planar or space steel truss, with a steel or concrete bottom plate, embedded within a concrete core which is cast in place. The beam is semi-prefabricate and it generally carries its own self-weight in Phase I, i.e., before the concrete casting, and then it collaborates with the concrete block as a unique system after casting and curing of concrete in Phase II. One of the most typical structural morphology of HSTCB is depicted in Fig. 1.

HSTCBs were introduced for the first time in Italy by Salvatore Leone, who was the inventor of a patent in 1967 and defined the first relevant production rules and calculation methods a few years later [1]. Similar typologies were also diffused abroad in the form of concrete composite truss beams, which were made of a concrete slab working with a steel joist, frequently adopted in the construction of bridges. However, this typology differed from that patented by S. Leone because the steel truss was not embedded within the concrete block.

After the introduction of HSTCBs by S. Leone, the development of HSTCBs followed several different directions, leading to the introduction of numerous diverse geometrical layouts in the construction industry. Since the beginning, it was clear that HSTCBs did not follow the same resisting and stress transfer mechanisms typical of RC and steel-concrete composite beams, but, in a certain measure, their mechanical behaviour was intermediate. Therefore, their adoption needed the repeated verification of the static performance of structural elements using design-by-testing procedures.

Today, these beams are extensively utilised in industrial buildings because of the benefits offered by the semi-prefabricated construction process and their capability to span large distances with minimal beam depths. Furthermore, in recent years, the scientific community has also directed its attention to studying the performance of HSTCBs in residential buildings, focusing on both static and seismic responses.

As mentioned before, the technical literature suggests that HSTCBs diverge from the mechanical principles governing RC or steel-concrete composite beams and, therefore, many efforts have been made in the last decades with the scope of achieving standardised design rules in national and international codes by fully understanding the main

* Corresponding author.
E-mail address: alessia.monaco@polito.it (A. Monaco).

https://doi.org/10.1016/j.istruc.2024.108018
Received 30 July 2024; Received in revised form 13 November 2024; Accepted 6 December 2024
Available online 18 December 2024

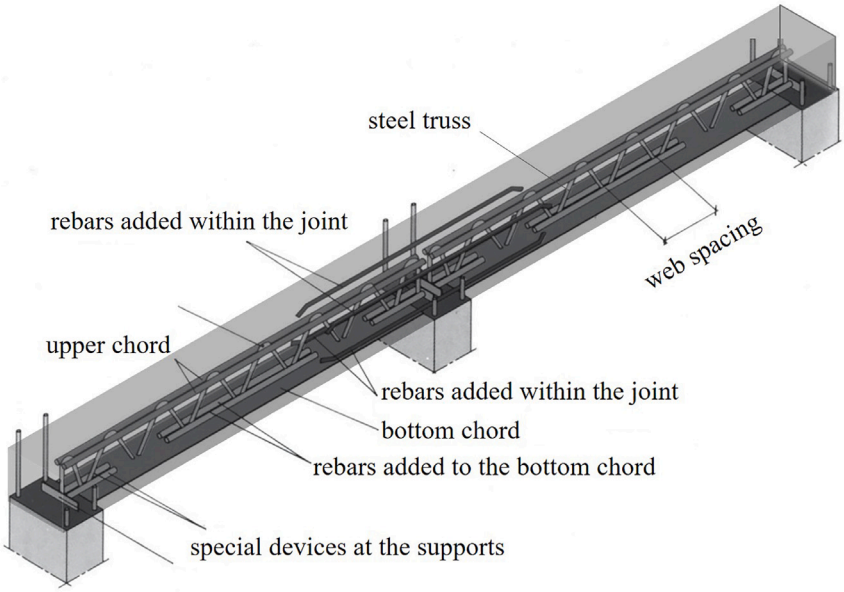

Fig. 1. Typical structural morphology of the HSTCB.

resistant mechanisms. Hence, recent research has sought specific insights into the distinctive structural behaviour of HSTCBs, particularly concerning flexure and shear, as well as their compliance with seismic requirements in earthquake-prone regions. One of the first deliverables which addressed this issue was represented by the guidelines provided in 2009 by the Italian Standard Commission for constructions concerning the procedures for the release of the authorisation to the usage of HSTCBs [2]. Later, a technical operational guide for the practitioners was published in 2011, which collected the results of a coordinated national research program conducted by several Italian Academies that conducted experimental campaigns and developed theoretical interpretations of the studied resistant mechanisms [3].

Within this framework, this review aims to synthesise the most noteworthy scientific findings gathered over the past twenty-five years by researchers both in Italy and internationally. The considered papers present the results of experimental campaigns on simply supported beams, beam-to-column joints, and specimens for analysing inner connections. Moreover, some of these papers present finite element numerical models developed for the detailed simulation of the strengthening mechanisms and contain the proposal of analytical formulation to provide design-oriented and code-compliant prevision models. Finally, after a careful synthesis of the main findings currently available, the literature review allows the detection of the lack of knowledge still remarkable, which mainly concerns the understanding of long-term performance and size-effect laws.

The paper develops as follows: Section 2 presents the bibliometric analysis of the database; Section 3 reports the main findings related to the response of the HSTCBs during the transient time of Phase I; Section 4 illustrates the experimental performance and some relevant prediction models of the mechanical behaviour of the HSTCBs in Phase II; Section 5 is devoted to the cyclic response of traditional and innovative joints including HSTCBs; Section 6 highlights the main currently open issues and gap of knowledge in the state-of-the-art, while conclusions are discussed in Section 7.

2. Bibliometric data from 1972 to today

This section reports the database of research papers, technical reports and guidelines on the design of HSTCBs from the 70's, produced in Italy and abroad. As Fig. 2a shows, 45% are journal articles, 43% are conference proceedings while remaining 12% are other documents,

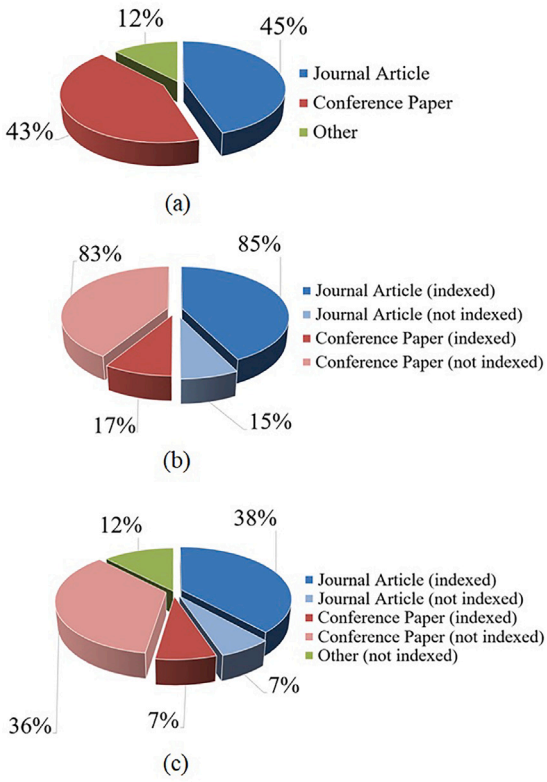

Fig. 2. Percentage of: (a) document type referred to the whole database; (b) Indexed/not indexed journal and conference papers referred to the total number of journal and conference papers; (c) Indexed/not indexed documents referred to the whole database.

i.e. technical reports and guidelines. Moreover, 85% of journal articles are Scopus-indexed while only 17% of conference papers are (see Fig. 2b). Also the documents classified as "other" are not indexed. Fig. 2c shows the percentage of indexed and not indexed documents considering the whole database. By analysing the database, it is interesting to observe the distribution of the documents during time reported in Fig. 3. In detail, from Fig. 3a it can be noted that very

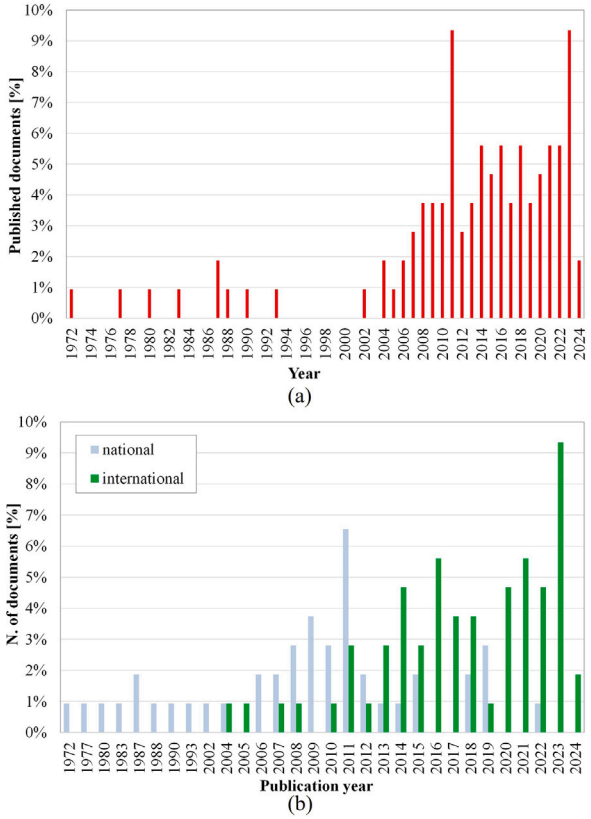

Fig. 3. Distribution of documents in percentage from 1972 to 2024: (a) whole database in time; (b) documents with national or international diffusion vs. publication year.

few investigations have been carried out until 2000's, when the scientific interest towards these beams started to increase after more than thirty years of practical adoption of this structural typology without specific guidelines. The growing attention to the design with HSTCBs is also demonstrated by the increasing international diffusion of the research results shown in Fig. 3b where the percentage of national and international documents is compared during the timeline. The database considered in this paper is analysed also considering the most relevant topic under investigation in each document. The main keywords are collected in Fig. 4 where the number of papers dealing with each topic is reported next to the corresponding bar. Considering the beam typology (Fig. 4a), there are documents in the database which focus on the behaviour of the beam during the first phase, i.e. before the concrete casting [3–16] and the second phase, i.e. after concrete casting, when the steel truss and the concrete material start to work as a composite system [3–5,9,10,12,14,15,17–83]. It can be noted that the behaviour in Phase II is more investigated than that in Phase I. Moreover, considering the two most diffused beam typologies, those with steel plate as bottom chord are more studied than the beams with reinforced concrete base. The plot also shows that most research focuses on beams with space steel trusses made of two parallel or inclined planar trusses [3,5,6,8,10–12,14,15,17,20,22–51,53–72,74–93], while only a few studies consider HSTCBs with single planar steel trusses [3,17,31,56,73,94]. Moreover, in some cases, the steel truss is made with ribbed steel, typical of RC beams [3,5,6,8,13,14,16,19,22–27,29,33,35,37–41,43,44,46–51,53–66,68–71,74–78,83,84], while in other cases, it is made of smooth steel, as the bottom steel plate is, when present [3,10,12,16,17,19,20,22,26,27,30–32,36–39,42,45,46,54,56,58,66,67,72,73,79–82,85–95]. Considering their mechanical response (Fig. 4b-c), HSTCBs are first of all analysed in order to understand the stress transfer mechanisms ruled by the inner connections. In the available literature, this investigation is mainly conducted by means of push-out

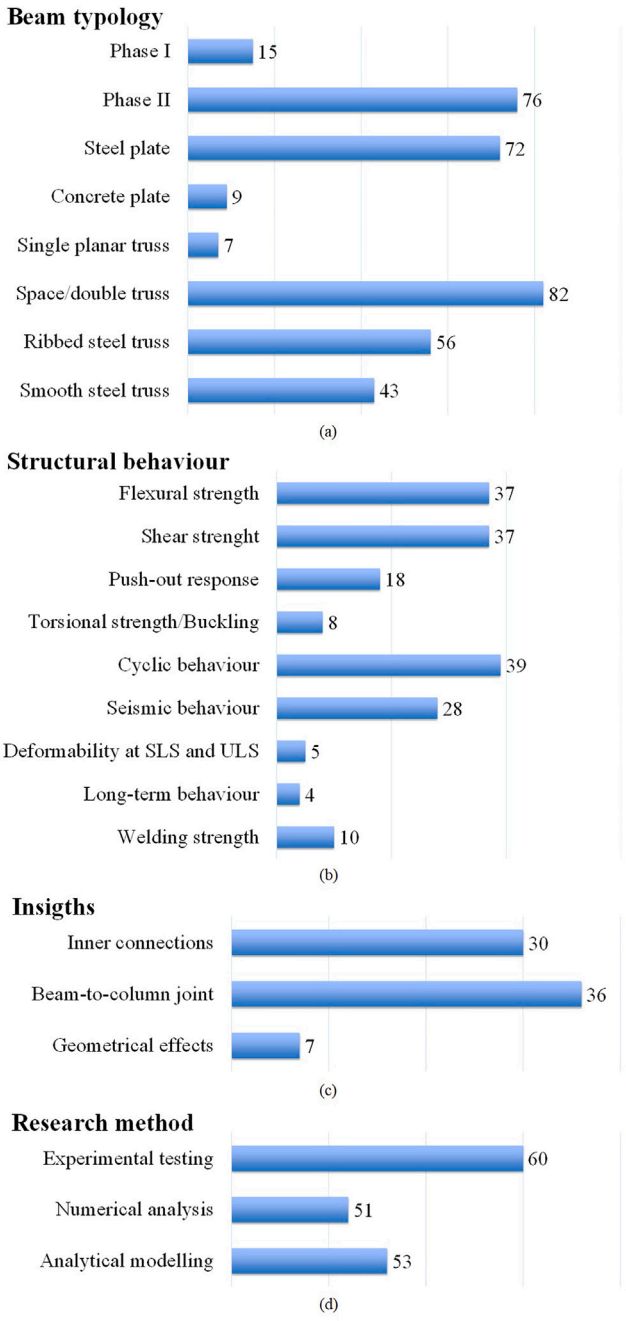

Fig. 4. Number of documents classified according to the most relevant keywords concerning: (a) beam typology, (b) structural behaviour, (c) insights, and (d) research method.

tests in Phase I and Phase II [3,5,14,17,20,22,27,28,37,38,43,46,54,56,58,66,73]. Many studies focus on both flexural and shear response in the second phase [3,4,6,7,9,10,12,15,18,19,23,25,26,29–31,34–37,39–42,44,45,47–49,51–53,55–60,65–67,79,84–93,95–98] and on the cyclic behaviour of joints which belong to civil constructions in seismic areas [3,12,23–26,32,33,35,44,50,56,57,60–64,68–72,74–78,80–84,90,94,99–104]. A smaller number of studies is available on other peculiar topics, such as the strength of the truss welds in the first and second phase [3,6,8,13,14,16,20,37,73], the torsional behaviour and buckling phenomena especially in Phase I [3,7,11,30,31,84,96], the deformability of the beams at Serviceability Limit State (SLS) and Ultimate Limit State (ULS) [29,31,42,86,88] and their long term behaviour [3,29,105]. The effect of geometrical parameters represents

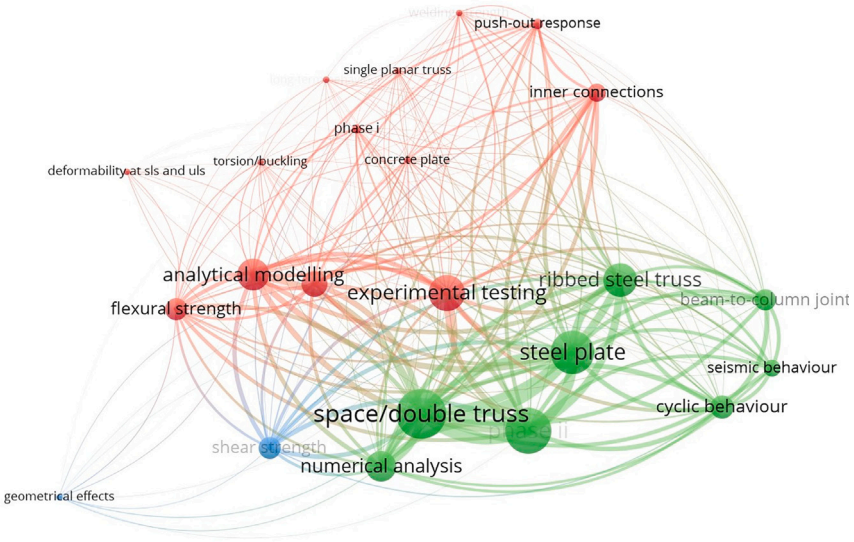

Fig. 5. Map of the most relevant linked keywords with higher co-occurrence. (Created with VOSviewer [106]).

a further insight in the considered database, where items such as the beam depth (i.e. full thick and slab thick beams), the diagonal bar slope, the spacing of the mesh, the depth-to-span ratios and the topological optimisation are investigated [7,15,53,65,89,91–93]. Considering the methodology, the documents report research results mainly obtained through experimental testing (about 56% of documents), numerical modelling developed with the Finite Element Method (FEM) (about 48% of documents) and analytical interpretation of the mechanical behaviour (about 50% of documents).

The most relevant keywords reported in Fig. 4 are also associated with a letter code from A to W in order to propose two synoptic tables in which the documents belonging to the analysed database are collected and linked to the main topics treated in the document. At the end of the document, Table R1 and Table R2 are provided. The first one collects the documents published between 1972 and 2015, while the second table those published between 2016 and 2024. In both tables, each document is associated with some letters which represent the following keywords: A - Phase I; B - Phase II; C - Steel plate; D - Concrete plate; E - Single planar truss; F - Space/double truss; G - Ribbed steel truss; H - Smooth steel truss; I - Flexural strength; J - Shear strength; K - Push-out response; L - Torsional strength/Buckling; M - Cyclic behaviour; *N* - Seismic behaviour; O - Deformability at SLS and ULS; P - Long-term behaviour; Q - Welding strength; R - Geometrical effects; S - Beam-to-column joint; *T* - Inner connections; U - Experimental testing; V - Numerical analysis; W - Analytical modelling.

Finally, Fig. 5 proposes a map aimed at better depicting the links between the most relevant keywords characterised by higher co-occurrence. The map was generated with VOSviewer [106]. The colours in the map indicate cluster of keywords which are linked to other keywords by means of curved lines that are visible if those keywords appear in the same document. Moreover, the thickness of the curve indicates the link intensity: thicker curves represent more frequent links, while thinner curves more rare links. As an insight of the analysis of linked keywords, the coloured circles in the map depict the keywords among all the relevant ones, which are characterised by higher levels of co-occurrence, indicating which are the most studied correlated topics.

From the analysis of this database, supported by the graphs and maps reported above, some items are chosen to be described more in detail in the following sections, which report the main findings taken from the most relevant research documents on that item.

3. Assessment of the behaviour in phase I

The behaviour of the beam in Phase I concerns the transient time during the construction process in which the steel truss is bare before the concrete casting. The analysis of the database, shows that the most relevant keywords with high co-occurrence with “Phase I" are those depicted in Fig. 6. In particular, considering the structural behaviour items, in this phase, one of the main problem is the buckling phenomenon of the compressed web bars or the upper chord of the steel truss. In the literature [3,7,11], three main different buckling modes have been identified: (1) the instability of the web truss or the upper chord, which involves the buckling length of a single rod; (2) the instability of the compressed upper chord with a buckling length that involves more than one mesh of the truss; (3) the coupled flexural–torsional instability of the steel truss. The classical criteria for investigating instability can be applied only in the first scenario, where the buckling length is determined by the distance between the transverse restraints of the upper chord or the length of the rods forming the web truss. However, if the transverse restraints are not rigid enough to prevent the displacement of nodes in the upper chord, this could lead to a collapse involving a buckling length that spans more than one mesh of the truss. Moreover, flexural–torsional instability could affect the entire beam, particularly in cases involving deep cross-sections. It is important to note that in these scenarios, the critical load value is significantly lower than the Eulerian critical load of individual rods. Nonetheless, it has been demonstrated that the critical load causing instability increases when the steel truss is configured as a spatial truss rather than a planar truss, thereby utilising both the axial and flexural strength of the diagonal web bars in the response mechanism.

3.1. Push-out response on bare specimens

To gain a better understanding of the behaviour of HSTCBs in Phase I, Badalamenti et al. [5] conducted monotonic push-out tests under displacement control on specimens constructed according to the scheme in Fig. 7.

This test was similar to the one recommended in Eurocode 4 [107] for push-out tests on classical composite steel-concrete beams. Two tests were performed on specimens S1 and S2. Specimen S1 consisted of two truss sections symmetrically joined along the bottom plate’s middle lines using an 8 mm thick connecting steel plate positioned perpendicular to the steel trusses’ plates. Each truss beam featured an upper chord of three coupled 16 mm diameter rebars, a bottom chord

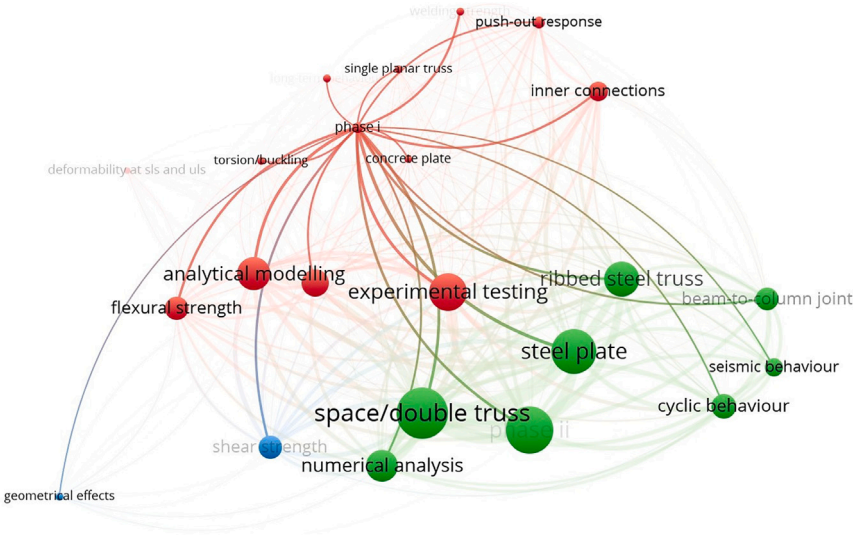

Fig. 6. Map of the keywords with higher co-occurrence with "Phase I". (Created with VOSviewer [106]).

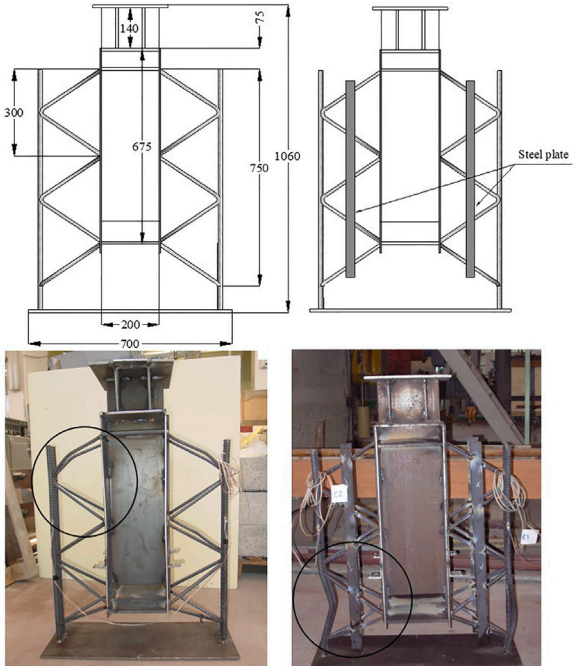

Fig. 7. Specimens for push-out test in Phase I (dimensions in mm) [5,14]: specimen S1 without vertical restraints (left) and specimen S2 with stiffeners (right).

of a 5 mm S355 steel plate, and B450C 12 mm diameter web rebars formed into a reverse V shape. The truss beam had a depth of 210 mm. An 8 mm thick plate was placed orthogonal to the specimen axis at the top and properly stiffened to apply the load through the testing machine. Specimen S2 differed from specimen S1 only by the addition of two longitudinal plates, each 40 mm wide and 5 mm thick. These plates were welded to the web bars to reduce their slenderness and prevent buckling. The specimens exhibited a similar peak resistance of 328 kN and 333 kN for specimen S1 and S2, respectively. The latter was analytically interpreted by Colajanni et al. [14], who calculated the moment-axial force domain of the diagonal bars of the specimens according to Eurcode 3 [108] and proposed a simplified mechanical model based on the static scheme reported in Fig. 8.

Considering the symbols in the figure, these equilibrium equations were written:

$$(N_1 - N_2)\sin\alpha^* - \frac{2}{l_w}(M_1 - M_2)\cos\alpha^* + \\ -\frac{1}{2l_c}\left(2(M_1 + M_2) + M_3 + M_4\right) = 0 \quad (1)$$

$$(N_3 - N_4)\sin\alpha^* - \frac{2(M_3 - M_4)\cos\alpha^*}{l_w} - \frac{3M_5}{l_c}\frac{\rho_{CB}}{\rho_{CB}+\rho_{CD}} + \\ +\frac{1}{2l_c}\left(2(M_1 + M_2) + M_3 + M_4\right) = 0 \quad (2)$$

$$S = \left(\sum_{i=1}^{5} N_i\right)\cos\alpha^* + \frac{2}{l_w}\left(\sum_{i=1}^{5} M_i\right)\sin\alpha^* \quad (3)$$

where ρ_{CB} and ρ_{CD} are the flexural stiffness of the rods labelled CB an CD, while l_w and l_c are respectively the length of the diagonal bar and the upper chord. The maximum external force S that the system can withstand was determined using the lower bound theorem of plasticity, as outlined by equilibrium equations Eqs. ((1),(2),(3)) and the allowable plastic and buckling conditions:

$$M_u = \frac{d^3}{6} f_y \left(1 - \frac{N_u^2}{N_y^2}\right) \quad (4)$$

$$\frac{N}{N^*} + \frac{M}{M^*} \leq 1 \quad (5)$$

In Eq. (4), d is the diameter of the rod, M_u and N_u are the ultimate bending moment and axial force, while N_y and f_y are the yielding axial force and tensile strength. Considering Eq. (5), $N^* = N_y$ in tension, while $N^* = N_b$ in compression, and M^* represents the yielding or plastic bending moment in the case of yielding domain or plastic domain, respectively. Consequently, the analytical estimate of the maximum load P was derived from the peak value of S, considering the interaction between the two trusses forming the beam. This yielded an estimated value of $P = 326.64$ kN, obtaining a ratio between predicted and experimental results of 0.996. Finally, the authors in [14] explained that a different mechanism was modelled for the failure of specimen S2 with the stiffening plates, which involved the buckling of the top chord. In a very simplified way, considering the reduced axial strength of the top chord, equal to N_b=66.5 kN, and considering that the latter was made of three rebars for each truss of the specimen, then the maximum load could be assessed as $P = 6 \cdot N_b = 399$ kN, with an overestimation of about 21%.

3.2. Welding strength

In order to integrate the analysis of the behaviour of HSTCBs during the first phase, the strength of welded joints is crucial. To this scope, several authors in the literature developed ad-hoc experimental tests on

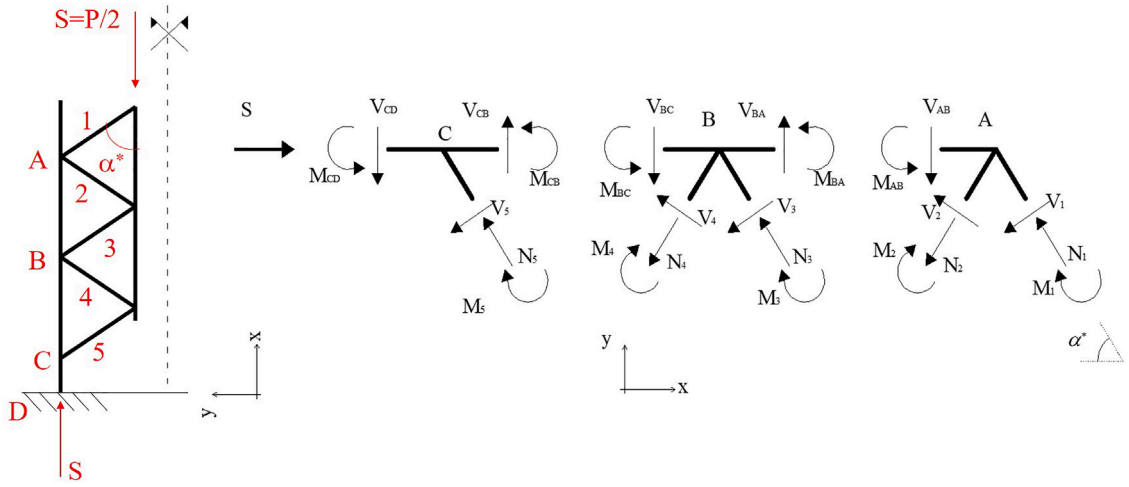

Fig. 8. Simplified mechanical model for pushout resistance in Phase I.
Source: Redrawn from [14].

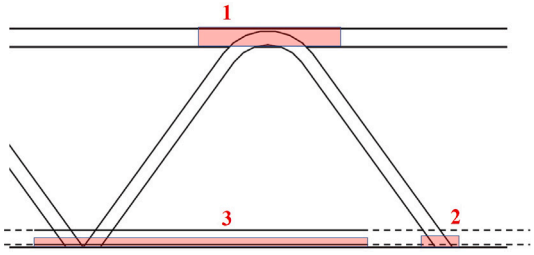

Fig. 9. Types of weld tested in Phase I.

fillet welds between two adjacent circular bars, i.e. the welds used to join the inverted V-shaped bars with the longitudinal upper chord (Type 1) [8,13,16], butt welds for the end-to-end joint between the diagonal web rebars and the steel plate (Type 2) [8,13] and fillet welds used to join the longitudinal rebars of the bottom chord to the steel plate (Type 3) [16]. These three types of weld are schematically depicted in Fig. 9.

For the Type 1 weld, two different specimens were prepared [8,16]; they are depicted in Fig. 10 and represent the weld between inverted V-shaped bars and longitudinal chord (Fig. 10a) and between two adjacent circular ribbed (Fig. 10b) and smooth (Fig. 10c) rebars. Similarly, Fig. 11 reports the other two typologies of welds [8,16].

The experimental results showed that the average welding strength of Type 1 specimens was about 57 kN according to La Mendola et al. [8, 13] while it ranged between 92–549 kN according to Caprili et al. [16]. Similarly, considering Type 2 specimens, La Mendola et al. [8] reported an average strength of about 65 kN. Finally, for Type 3 welding, Caprili et al. [16] obtained a range of variation of the strength similar to that of Type 1 specimens, i.e. between 95–535 kN. In all cases, different failure modes were observed, involving the bar or the welding failure. The authors in [8,13,16] also proposed the analytical interpretation of the failure load according to the following equations [108]:

$$f_{vw} = \frac{f_u}{\beta_w \sqrt{3}} \tag{6}$$

in which f_{vw} is the welding strength, f_u is the nominal ultimate stress of the filler metal and β_w is the correlation factor for the fillet welds, equal to 0.9 for all specimens tested in [8,16]. In particular, for specimens of Type 1 and 2 tested in [8], the average ratio between experimental and analytical failure load was about 1.137 and 1.253 respectively.

As the main conclusion, these studies showed the reliability of welded joint fabrication techniques; however, tests have shown that the use of stronger filler material did not always guarantee higher weld strength, as the welding execution methods played a decisive role, which could result in a different throat section height.

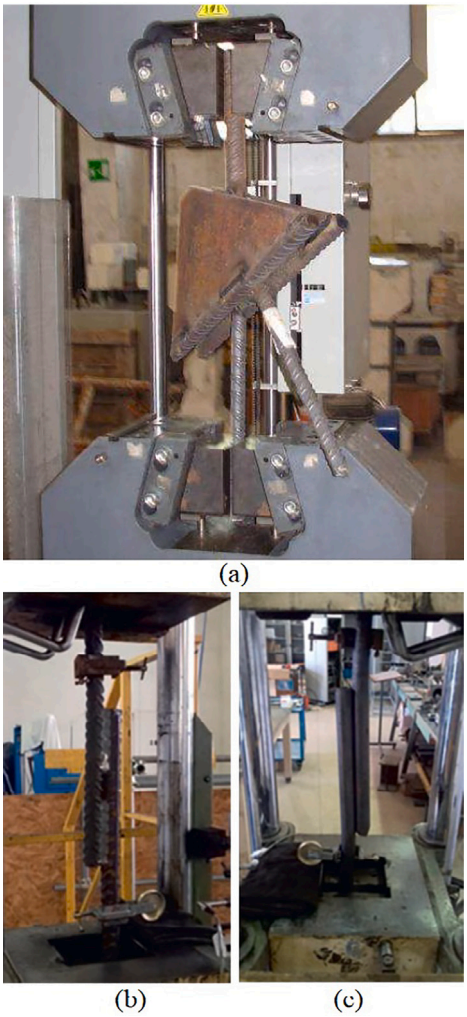

Fig. 10. Specimens of Type 1 weld tested by: (a) La Mendola et al. [8]; (b) and (c) Caprili et al. [16].

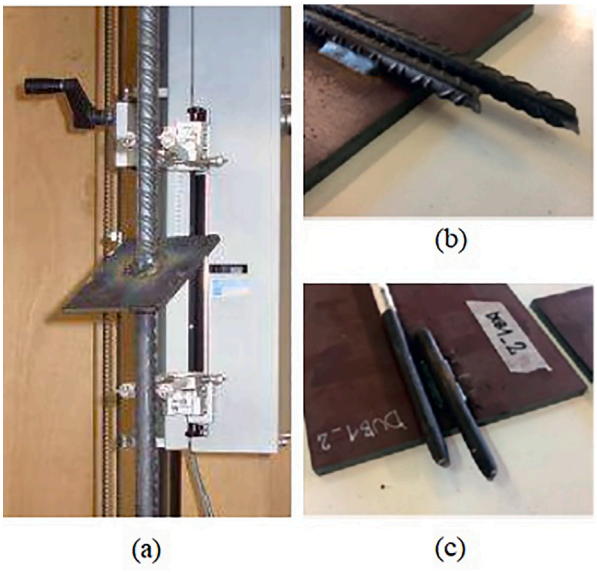

Fig. 11. Specimens of weld of: (a) Type 2 [8]; (b) Type 3 with ribbed bars [16]; (c) Type 3 with smooth bars [16].

4. Structural performance during phase II

This section presents several investigations conducted in the literature on the mechanical behaviour of HSTCBs during the second phase, i.e. after the concrete casting and curing. Fig. 12 shows the most relevant topics studied in relation to Phase II behaviour, which are predominantly related to the stress transfer mechanisms and the flexural and shear resistance. Most studies refer to HSTCBs with a bottom steel plate and a ribbed steel truss, and they are predominantly conducted through experimental tests, with subsequent analytical and/or numerical interpretation of the results. This section specifically addresses local slip issues related to the stress transfer mechanism, showcasing the results of Phase II push-out tests conducted by various authors [14,17,22,37,73]. Additionally, it describes experimental analyses focused on these beams' global flexural and shear behaviour [36,39,45,55].

4.1. Analysis of the stress transfer mechanisms

Push-out tests are the first experimental method useful for investigating stress transfer mechanisms. They have been conducted on HSTCBs since the '80s by reproducing the same testing technique adopted for classical composite beams according to Eurocode 4 [107]. As in traditional push-out tests, two identical trusses are connected using a steel plate welded perpendicular to the bottom chords of the trusses, and this plate is reinforced at the load application point. The bars used in these tests can be made of ribbed or smooth steel, and the trusses can be single or double. This section considers the push-out tests conducted by Puhali and Smotlack [17] in 1980; Aiello [22], Tullini and Minghini [37] and Colajanni et al. [14] between 2009 and 2014 and, more recently, by Vigneri et al. [73] in 2022. The specimens tested by these authors are depicted in Fig. 13.

Puhali and Smotlack [17] prepared specimens with both planar and space trusses, made with a 6 mm thick steel plate as the bottom chord and web bars and upper chord characterised by the same diameter, which was between 14 mm and 32 mm. They adopted smooth steel of class S355, while the concrete compressive strength was in the range 26–30 N/mm^2. The authors observed that the specimens with a space truss (B-P4, B-P5, and B-P6) performed with higher stiffness and strength compared to the samples with planar truss (A-P1, A-P2, and A-P3); moreover, the specimens with web bars with smaller diameter (A-P1 and B-P4) demonstrated lower strength but a more ductile response. Specimens with larger diameter web bars showed greater strength but underwent a more brittle failure mechanism characterised by concrete failure or buckling of the steel plate. Aiello [22] tested eight specimens: S12-# samples were made with smooth steel (class S355) diagonal bars with diameter 12 mm, while in S14-# samples the diameter was 14 mm; similarly, specimens B12-# and B14-1 were made of ribbed steel (class B450C) and were characterised by 12 mm and 14 mm diameter web rebars, respectively. In all specimens, the upper chord was an 18 mm diameter web rebar made of ribbed steel of class B450C, while the bottom chord was a 6 mm thick steel plate (class S355). The average concrete compressive strength was about 43 N/mm^2. In nearly all cases, the collapse of the specimens was due to concrete failure; however, welding failure also occurred occasionally. The specimens exhibited an overall ductile response until failure. Tullini and Minghini [37] tested three identical specimens. The truss was constructed using an S355 steel plate with a thickness of 4 mm, 12 mm diameter web bars, and an 18 mm diameter upper chord. The bars were made of steel with a nominal yield stress of 440 N/mm^2, and the concrete had an average compressive strength of about 42 N/mm^2. The ultimate load was reached prematurely in all tests due to welding failure. Colajanni et al. [14] tested three identical specimens, too, with a double space truss made of B450C steel; the diameter of the web rebars was 12 mm, and the bottom plate was 5 mm thick and made of steel class S355. The average concrete compressive strength was about 28 N/mm^2. For all specimens, failure occurred when the concrete reached its tensile strength, resulting in large longitudinal cracks. These cracks progressively transferred tensile stresses from the concrete to the tensile web bars of the steel trusses, causing significant plastic deformation near their connection to the plate. Finally, in more recent years, Vigneri et al. [73] conducted further push-out tests on specimens with planar trusses (single truss or two parallel planar trusses), made of smooth steel of class S355. The geometry of these specimens differed from the previous ones because the transversal cross-section was wider: in fact, Vigneri et al. [73] wanted to simulate the steel truss embedded within a concrete slab instead of a concrete beam. They also used two concrete classes, i.e. C25/30 and C45/55. Another distinctive feature of this experimental campaign was given by the preparation of two additional types of specimens, labelled with B and C, that differed from the A typology (depicted in Fig. 13) because they were made only with a cut sinusoid with or without two additional bottom chords welded to the steel plate. The main failure modes observed in these tests were the concrete crushing and pull-out.

Table 1 summarises the results obtained in the considered literature. The detected failure modes are indicated in the table through the following codes: C, Concrete crushing; CP, Concrete Pull-Out and crushing; SW, Steel Web strength; SP, Steel Plate buckling; W, Welding failure. Moreover, the ultimate loads reported for the specimens tested by Tullini and Minghini [37] and Vigneri et al. [73] are indicated with an asterisk because the values refer to the maximum load carried per weld.

Two main analytical models should be mentioned for the interpretation of the push-out response. The first one was proposed by Colajanni et al. [54], who considered the plastic behaviour of the inclined web bars of the beam as the ruling mechanism. The model was governed by five primary parameters explained below. (1) The slope α of the diagonal bars in the 3D space, which act as the dowels of the system:

$$\alpha = \arccos\left(\frac{0.5\,s}{\sqrt{0.25\,s^2 + d^2 + 0.25\,b^2}}\right) \tag{7}$$

where s, b and d are the lattice spacing, width and depth, respectively;

(2) the bearing stress of concrete f_b:

$$f_b = \psi \cdot f_c \tag{8}$$

where ψ is a coefficient that rules the value of the plastic strength of concrete f_c when it is fully confined, and that depends on the concrete cover [109];

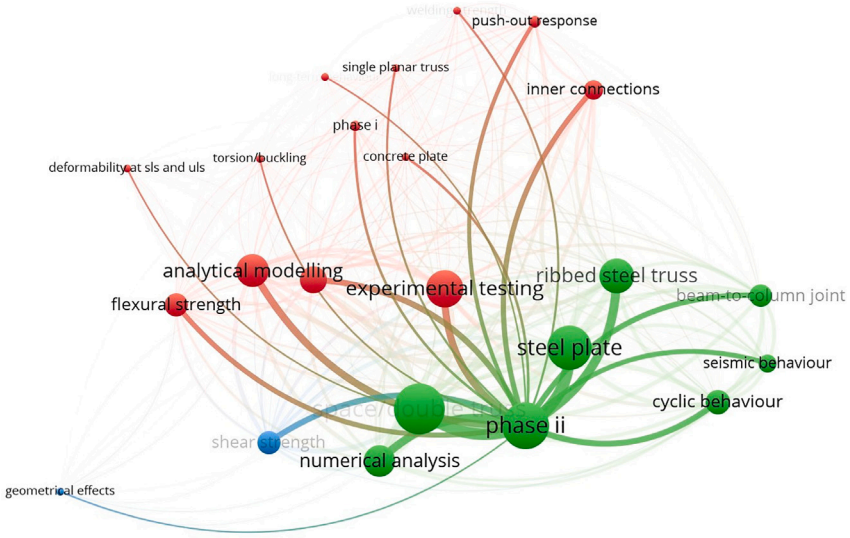

Fig. 12. Map of the keywords with higher co-occurrence with "Phase II". (Created with VOSviewer [106]).

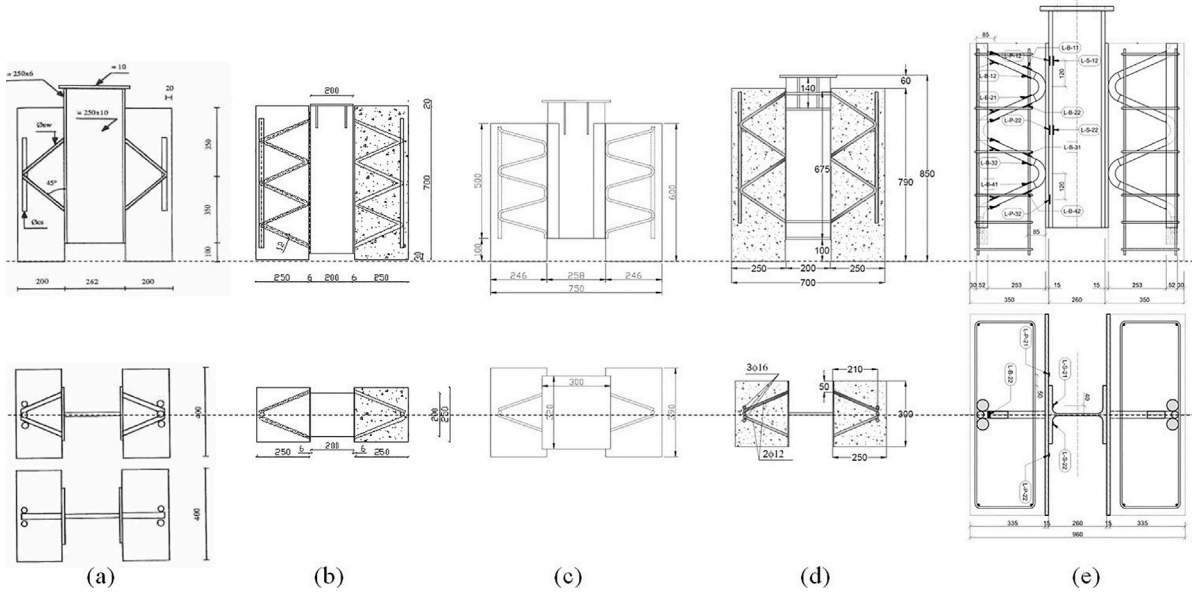

Fig. 13. Push-out tests in Phase II conducted by: (a) Puhali and Smotlack [17]; (b) Aiello [22]; (c) Tullini and Minghini [37]; (d) Colajanni et al. [14]; (e) Vigneri et al. [73]. (Dimensions in mm).

(3) the distance between the two plastic hinges in the dowel $L_{eff}-a$, which is calculated as the effective length, L_{eff}, minus the length of the plastic hinge located in the proximity of the steel plate, a;

(4) the plastic bending moment M_{pl} in the $M-N$ domain according to Millard and Johnson [110]:

$$M_{pl} = \frac{d_w^3}{6} f_y \left(1 - N^2 \Big/ \left(\pi \frac{d_w^2}{4} f_y\right)^2\right) \tag{9}$$

(5) the shear-normal stress interaction $M-N-V$ according to Eurocode 3 [108], which takes into account the reduction coefficient ρ:

$$\rho = (2V / \left[(0.8 f_u A_{sw}) - 1\right])^2 \tag{10}$$

with f_u the ultimate strength of the steel bar with cross section area A_{sw}.

The solving equation proposed by the authors [54] can be finally written as:

$$V^2 \left(\frac{\sin^2\alpha}{2 f_b d_w} + \frac{16\cos^2\alpha}{3\pi^2 d_w f_y \left(1 - \left(\frac{10V}{f_u \pi d_w^2} - 1\right)^2\right)} \right) - V \cdot a \cdot \sin\alpha + \\ - \left(\frac{d_w^3}{3} f_y \left(1 - \left(\frac{10V}{f_u \pi d_w^2} - 1\right)^2\right) - \frac{f_b d_w a^2}{2} \right) = 0 \tag{11}$$

Moreover, two simplified expressions were proposed. The first one was obtained by neglecting the $M-N-V$ domain:

$$V^2 \left(\frac{\sin^2\alpha}{2 f_b d_w} + \frac{16\cos^2\alpha}{3\pi^2 f_y d_w} \right) - V \cdot a \cdot \sin\alpha + \\ - \left(\frac{d_w^3}{3} f_y - \frac{f_b d_w a^2}{2} \right) = 0 \tag{12}$$

Table 1
Results of push-out tests in Phase II from literature.

Author	ID	d_w [mm]	P_u [kN]	failure
Puhali and Smotlack [17]	A-P1	14	463	SW
	A-P2	24	648	C
	A-P3	32	844	C
	B-P4	14	736	SW
	B-P5	24	1178	C
	B-P6	32	1325	SP
Aiello [22]	S12–1	12	817	C
	S12–2	12	842	C
	S14–2	14	787	C
	S14–3	14	808	C
	S14–4	14	861	W
	B12–1	12	996	C
	B12–2	12	1008	W
	B14–1	14	1139	SW
Tullini and Minghini [37]	S1	12	61*	W
	S2	12	63*	W
	S3	12	71*	W
Colajanni et al. [14]	P1	12	1052	C
	P2	12	1005	C
	P3	12	1258	C
Vigneri et al. [73]	D32-1-C25-A	32	609*	C
	D32-1-C45-A	32	680*	C
	D20-1-C25-A	20	287*	C
	D20-1-C45-A	20	308*	C
	D20-2-C25-A	20	278*	C
	D20-S125-C25-A	20	301*	C
	D32-1-C25-B	32	318*	CP
	D32-2-C25-B	32	267*	CP
	D32-3-C25-B	32	199*	CP
	D32-1-C25-C	32	169*	CP
	D20-1-C25-C	20	91*	CP

The last simplified expression was obtained by ignoring also the distance a, thus achieving an analytical expression for the dowel strength V, useful for practical applications:

$$V = \frac{d_w^2\sqrt{2 f_y f_b}}{\sqrt{3\sin^2\alpha + \frac{32 f_b}{\pi^2 f_y}\cos^2\alpha}} \tag{13}$$

In Colajanni et al. [54], the analytical formulation was then verified against some experimental results of push-out tests [14,17,22,37] and several FEM analyses conducted by the same authors, reporting the following average ratio between the analytical prediction P_{theo} and experimental value P_{exp}:

- $P_{theo}/P_{exp} = 1.01$ ($CV_r = 0.20$) when using Eq. (11);
- $P_{theo}/P_{exp} = 1.05$ ($CV_r = 0.24$) when using Eq. (12);
- $P_{theo}/P_{exp} = 0.91$ ($CV_r = 0.21$) when using Eq. (13).

More recently, Vigneri et al. [73] developed a reliability analysis for obtaining the expression of the longitudinal shear strength resistance function in HSTCBs. The authors observed the similarities of this system with that of headed stud shear connectors, especially in terms of combined concrete crushing and steel bending failure. Therefore, their initial reference formulation corresponded to that given in Eurocode 4 [107] for predicting the shear resistance of studs in solid slabs due to concrete crushing. Considering the features of the specimens previously tested in their experimental campaign [73], they calculated the longitudinal shear resistance for each bottom weld between sinusoidal web bars and base plate. Moreover, they remarked on the difference between the expected resistance depending on the type of specimen (Type A, B and C previously described), and therefore, they introduced a reduction factor $k_{w,type}$ that takes into account the type of sinusoid (complete or cut, with/without added bottom bars):

- $k_{w,type} = 1.0$ (Type A specimens);
- $k_{w,type} = 0.53$ (Type B specimens);
- $k_{w,type} = 0.26$ (Type C specimens).

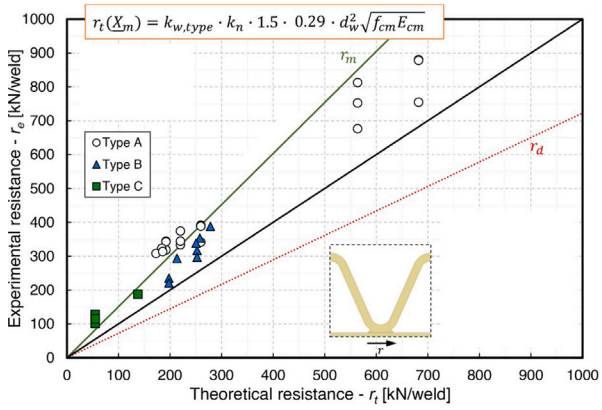

Fig. 14. Comparison between theoretical and experimental resistance according to Vigneri et al. [73].
Source: Redrawn from [73].

The authors also considered the interaction between the number of parallel sinusoids, n_r, placed at a centre-to-centre distance equal to s_t, by formulating a reduction coefficient k_n:

$$k_n = \frac{\left(5 \cdot k_s - 4\right) \cdot \left(n_r - 2\right) + 2 \cdot k_s}{n_r} \tag{14}$$

where

$$k_s = 0.9 + \frac{0.1\left(s_t - d_w - d_c\right)}{5 d_w - d_c} \le 1 \tag{15}$$

with $s_t \ge d_w + d_c$.

In Eqs. (14) and (15), d_w and d_c are the nominal diameter of the diagonal bars and chords, respectively.

From the equations above, and using the mean values of the basic variables X_m, the following resulting expression was obtained for the resistance function $r_t(X_m)$:

$$r_t(X_m) = 1.5 \cdot k_{w,type} \cdot k_n \cdot 0.29 \cdot d_w^2\sqrt{f_{cm}E_{cm}} \tag{16}$$

In Eq. (16), the terms f_{cm} and E_{cm} are the mean values of the cylinder strength and secant modulus of elasticity of concrete, respectively.

Fig. 14 shows the validation of this analytical model to the experimental database [73]. The authors obtained a linear correlation coefficient of 0.979 and a coefficient of variation $CV_r = 0.213$, demonstrating a good agreement between theoretical prediction and experimental evidence.

The same figure proposes the trend of the design value of the longitudinal shear resistance r_d that the authors finally proposed by distinguishing the contribution given by the lower parts of the sinusoidal diagonals and the top weld between sinusoidal webs and chords. To the scope, they introduced two coefficients, i.e. k_{bot} and k_{top}, respectively, and obtained the following design expression:

$$P_{rd} = \frac{\left(k_{bot} + k_{top}\right) \cdot k_n \cdot 0.29 \cdot d_w^2\sqrt{f_{ck}E_{ck}}}{\gamma_v} \tag{17}$$

in which f_{ck} and E_{ck} are the characteristic values of the cylinder strength and secant modulus of elasticity of concrete, respectively, and the recommended value for γ_v is 1.25. Finally, the suggested values for k_{bot} and k_{top} are given according to the following cases:

- $k_{bot} = 1.0$ (bottom chords, with steel plate underneath);
- $k_{bot} = 0.5$ (no bottom chords, with steel plate or "carter" underneath);
- $k_{top} = 0.0$ (full utilisation of vertical shear resistance);
- $k_{top} = 0.5$ (reduced vertical shear resistance needed).

As a final note, the authors reported that $k_{top} = 0.5$ may be adopted only if the full plastic capacity of the diagonal is reduced by 15%; otherwise, further advanced analysis should be conducted to assess the coefficient more accurately.

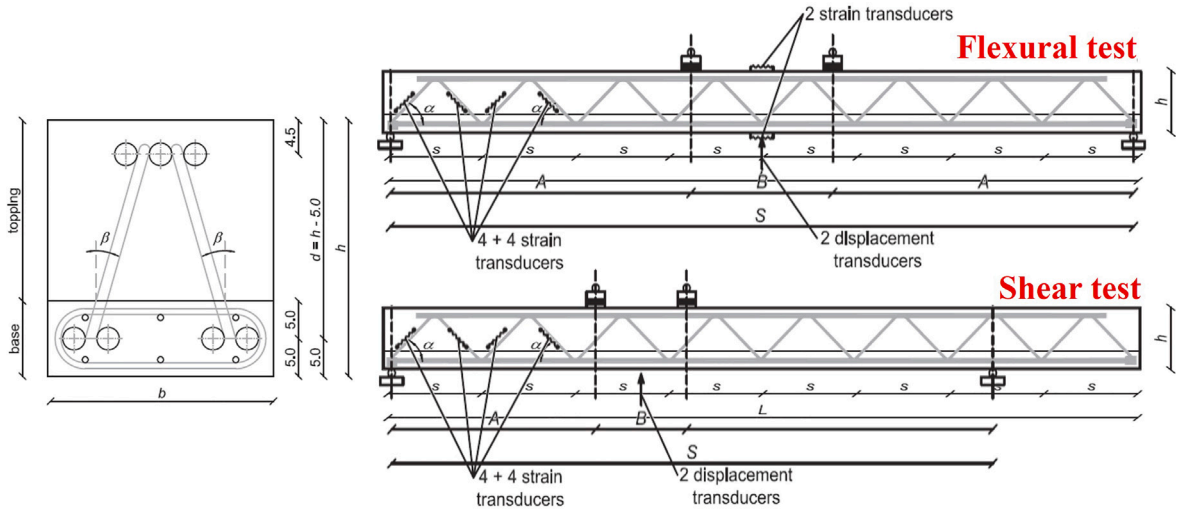

Fig. 15. Specimens tested by Tesser and Scotta [36] (dimensions in cm).
Source: Redrawn from [36].

4.2. Bending and shear

In the literature, there are several tests aimed at understanding the behaviour of HSTCBs in flexure and shear. Generally, the studies start from the execution of experimental tests, which are then interpreted using analytical and numerical models. In this section the most relevant tests on HSTCBs in Phase II are briefly summarised. In detail, the experiments conducted by Tesser and Scotta [36], Chisari and Amadio [39], Monti and Petrone [45] and Colajanni et al. [55] are considered.

Tesser and Scotta [36] performed the tests on HSTCBs with inferior precast base surrounding the bottom chord of the steel truss. Moreover, they designed the beams in order to apply to each specimen two different tests, inducing, firstly, a flexural failure and, secondly, a shear failure (Fig. 15).

The specimens had a length L of about 6 m and different cross sections with the base b equal to 0.25 m, 0.3 m or 0.4 m and the depth h equal to 0.24 m, 0.34 m, 0.44 m or 0.54 m. The top chord was made of three bars of smooth steel (class S355JR) with diameter equal to 26 mm, 28 mm or 30 mm, while the bottom chord was made with four bars of diameter 28 or 30 mm embedded within the concrete base. The steel truss was made with diagonal bars of diameter 14 mm or 16 mm. The spacing between the meshes varied between 0.40 mm and 0.46 mm. Different inclinations were chosen for the angles α and β indicated in Fig. 15. The concrete class was C50/60, i.e. characteristic cylindrical compressive strength equal to 50 MPa. All the details of each specimen are available in [36]. Table 2 reports the maximum loads attained by the specimens in flexural tests ($P_{max,flex}$) and shear tests ($P_{max,shear}$).

The crack pattern observed in the flexural tests was characterised by cracks wider than 0.5 mm, generally opened in the central sections of the beam, with a sub-vertical direction going from the concrete base to the concrete topping. All beams exhibited yielding in the lower chord across the range of section sizes and longitudinal reinforcement ratios tested. Additionally, specimens B3 and B6 experienced concrete crushing in the upper part of the section between the two load application points. The crack pattern observed in the shear tests was characterised by at least one diagonal crack between the support and the nearest loading axis in the upper concrete section. This crack progressively widened, extending at one end towards the upper section edge and at the other towards the interface between concrete casts. Subsequently, in this latter direction, the cracks advanced horizontally along the interface towards the closest support, except in beam B8. At peak strength, two phenomena were observed either together or separately. First, the crack at the interface enlarged and moved towards the support, often causing detachment of the concrete base near the end of the lower chord. Second, the interface cracks continued diagonally in the concrete base, typically offset from the concrete topping. In all cases, the shear test cracks did not intersect with the flexural test cracks.

Table 2
Flexural and shear resistance of the specimens tested by Tesser and Scotta [36].

ID	$P_{max,flex}$ [kN]	$P_{max,shear}$ [kN]	Error flex [%]	Error shear [%]
B1	111	149	−9.7	24
B2	150	192	−21.4	4
B3	143	263	−21.4	−22
B4	211	293	−6.4	2
B5	208	382	−7.7	−18
B6	193	280	−15.2	15
B7	276	490	−17.5	−22
B8	313	496	−9.9	−16
B9	303	501	−4.2	−10
B10	332	457	−10.4	5
B11	326	376	−6.8	17
B12	328	381	−9.2	23
Average			−11.6	0
St. Dev.			5.8	17

For the analytical interpretation of the results, the authors in [36] adopted two analytical formulations. The flexural capacity M_{Rd} was assessed according to Eurcode 2 [111]:

$$M_{Rd} = f_y A_s d \left(1 - \frac{a}{d}\frac{x}{d}\right) \tag{18}$$

$$\frac{x}{d} = \frac{\frac{\sigma_s}{f_y}A_s - \frac{\sigma'_s}{f_y}A'_s}{\beta_r f'_c b_{eff} d} \tag{19}$$

where A_s and A' are the tensile and compressive steel reinforcement, respectively, while σ_s and σ' are the corresponding stresses; d is the effective depth of the beam, f'_c the concrete cylindrical compressive strength, b_{eff} the effective compressive concrete width, and β_r a coefficient for the integration of the stress distribution over the section (equal to 0.8 if the stress block simplification is assumed).

For the assessment of the shear capacity, the authors proposed several models from existing building codes. For brevity, only the expressions given by Model Code 2010 [112] are reported because they proved to be more accurate in predicting the experimental data. The authors in [36] assumed that the nominal shear strength can be estimated as the sum of concrete and steel contributions:

$$V_{Rd} = V_{cRd} + V_{sRd} \tag{20}$$

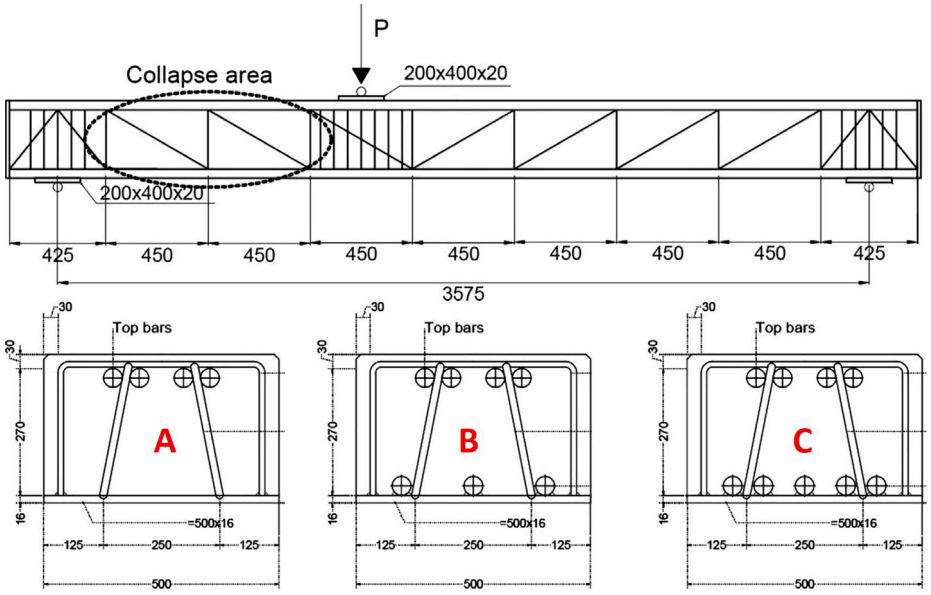

Fig. 16. Specimens tested by Chisari and Amadio [39] (dimensions in mm).
Source: Redrawn from [39].

$$V_{cRd} = k_v b z \sqrt{f'_c} \tag{21}$$

$$V_{sRd} = A_{sw} f_{yw} (\cot \vartheta + \cot \alpha) \sin \alpha \cdot \cos \beta \cdot z/s \tag{22}$$

In Eq. (20), Eq. (21) and (22), k_v is a coefficient depending on the concrete compressive strength, in the range 0.145 - 0.178 for the tested beams; z is the inner lever arm of the section; A_{sw} and f_{yw} are the area and yield strength of the transversal reinforcement, respectively; ϑ indicates the inclination of the compression strut to the beam axis.

The comparison between experimental and theoretical results is reported in Table 2 in terms of the errors given by the validation. More in detail, for each specimen, for the flexural capacity, the error is assessed as:

$$Error\ flex = \frac{M_{rd} - M_{\exp}}{M_{\exp}} \% \tag{23}$$

and similarly, in shear it is assessed as:

$$Error\ shear = \frac{V_{rd} - V_{\exp}}{V_{\exp}} \% \tag{24}$$

The second experimental campaign considered in this section was performed by Chisari and Amadio [39] on nine specimens of HSTCBs with bottom steel plate. The authors performed three-point bending tests with shear failure. The reinforcement details and the static scheme of tests are reported in Fig. 16.

All specimens had a 16 mm thick steel plate, grade S355, and steel reinforcement made with smooth steel (specimens A3, B3 and C3) or ribbed steel (specimens A1, A2, B1, B2, C1 and C2), class B450 C and S355, respectively. The top reinforcement was made with four ribbed bars with a diameter of 40 mm, while the bottom reinforcement, when present, was made with three or five rebars with the same diameter. The web reinforcement was constituted by a couple of diagonal rebars with a diameter of 16 mm at a spacing of 450 mm, made of smooth steel (specimens A2, B2 and C2) or ribbed steel (all other specimens). The average concrete compressive strength was about 47 N/mm^2. The experimental results are summarised in Table 3.

The test results showed that different steel trusses do not significantly change the overall shear capacity of the beam; generally, specimens made with ribbed steel exhibited higher stiffness and ultimate strength. They also observed that the higher the number of bottom rebars, the greater the first-cracking load, allowing a better serviceability limit state performance. Without the bottom bars, the steel base and concrete bond were maintained solely by the joist and the vertical external plates, and the plate itself was essentially smooth. This resulted in poorer performance at both the serviceability and ultimate limit states. However, when bottom bars were present, they helped to sustain a minimum bond. In general, almost all specimens exhibited an overall ductile failure. No welding failures were observed after the concrete was removed. Inclined cracks appeared in the concrete in all cases, accompanied by a concurrent slip between the steel plate and the concrete. In some instances, the inclined cracks merged with debonding cracks, but generally, the debonding cracks remained stable, and the collapse was caused by the propagation of the inclined cracks. Due to the presence of the steel truss, longitudinal cracks also appeared in the upper part of the beams, separating the inner concrete from the outer section.

Table 3
Test results obtained by Chisari and Amadio [39].

Specimen ID	A1	A2	A3	B1	B2	B3	C1	C2	C3
$P_u[kN]$	861	865	856	1078	929	931	1048	975	1027

Chisari and Amadio [39] also proposed several numerical and analytical interpretations of the shear failure mechanism. In particular, they considered an additive model in which the shear resistance V_{Rd} is the sum of two contributions, given by the concrete panel zone, subjected to diagonal compression, V_{Rcd}, and the steel reinforcement, V_{Rsd}. The authors proposed the resolution of the hyperstatic scheme of the concrete panel reinforced with steel ties, and, deducing some parameters from their numerical simulations, suggested these equations:

$$V_{Rcd} = \frac{f'_c f_{ct}}{0.66 f'_c + 1.99 f_{ct}} bh \tag{25}$$

$$V_{Rsd} = \left(A_{sw} f_{yw} - \frac{V_{Rcd}}{\sin \alpha} \frac{1}{k_2 \left(\frac{1}{k_1} + \frac{a}{E A_{sw} \cos \alpha} \right)} \right) \sin \alpha \tag{26}$$

In Eq. (26), the coefficients k_1 and k_2 are equal to $k_1 = 0.963 G b \sin \alpha$ and $k_2 = k_1 \left(\frac{1}{\left(\frac{s}{h} - 0.628 \right)^2} + 1 \right)$. Moreover, f_{ct} is the tensile strength of the concrete and h the lever arm, which can be approximated by the steel joist height. The proposed model was validated by the authors

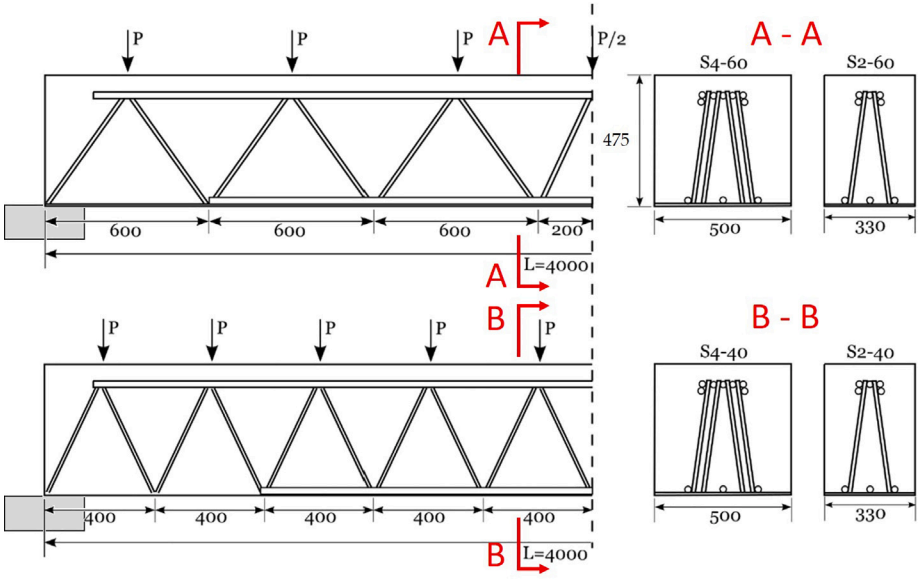

Fig. 17. Specimens tested by Monti and Petrone [45] (dimensions in mm).
Source: Redrawn from [45].

Table 4
Test results obtained by Monti and Petrone [45].

Specimen ID	$V_{y1}[kN]$	$V_{y2}[kN]$	$V_{max}[kN]$ (from [79])
S2–60	270	400	450
S2–40	516	571	650
S4–60	500	–	812
S4–40	751	879	900

considering the wide numerical database that they obtained through several parametric analyses: they obtained a very good correlation with the numerical ultimate loads, achieving an average error of −0.92% and a standard deviation of 11.06%.

A similar experimental campaign was conducted by Monti and Petrone [45] on four full-scale beams, whose details are depicted in Fig. 17. In particular, these tests were aimed at examining the effects of diagonal reinforcement quantity and spacing.

Each specimen measured 4 m in length, was simply supported, and subjected to point loads applied above the top nodes of the reinforcing truss. All beams had a cross-sectional depth of 475 mm, with a vertical centre-to-centre distance of 400 mm between bottom and top chords. Specimens S2–40 and S2–60 had a cross-sectional width of 330 mm; their steel reinforcement was made with a space truss with a 330 × 8 mm bottom steel plate, a top chord with five 30 mm bars, and two diagonals with a diameter of 16 mm, spaced at 400 mm (S2–40) or 600 mm (S2–60). Conversely, specimens S4–40 and S4–60 had a cross-sectional width of 500 mm, a 500 × 10 mm bottom steel plate, a top chord made with seven bars with a diameter of 32 mm, and four diagonals with a diameter of 16 mm, spaced at either 400 mm (S4–40) or 600 mm (S4–60). The steel adopted was a smooth steel with a characteristic yielding strength of 334.5 N/mm^2 while the characteristic concrete compressive strength was 41.2 N/mm^2. The results of the tests are summarised in Table 4. In particular, it can be noted that the authors reported two main shear resistance values, denoted as V_{y1} and V_{y2}, which represent the value of the shear capacity at yielding of the first web steel bar and at yielding of the second web steel bar, respectively. Conversely, the values of the total shear capacity of the specimens was assessed from the force–displacement curves [79].

As a test result, the authors monitored the relationship between the strain in the tensile diagonal bars and the increasing shear value, observing that the first couple of tensile bars yielded before the second one, confirming their hypothesis of a failure sequence of the shear-resisting elements. Moreover, from the crack pattern of specimen S2–60 after increasing the load beyond flexural failure, they also observed that the concrete strut actually formed.

The authors remarked on the importance of the shear capacity related to the number of couples of diagonals reaching the yielding because they formulated an analytical model under this assumption. This modelling approach allowed the tracking of the development of shear capacity as yielding progressed from the initial pair of web steel bars to the subsequent pairs, provided that the concrete did not crush. To the scope, the following simplified code-compliant equation was proposed:

$$V = \kappa f_{yw} A_{sw} \sin\alpha \tag{27}$$

with

$$\kappa = \frac{n_t - 2(1-\delta_p)}{n_t - 2(n_s - \delta_p)} \tag{28}$$

In Eq. (28) n_t is the overall number of tensile web steel bars of the beam; $n_s = n$ is the number of tensile web bars that yield; δ_p is a coefficient equal to 0 if the load is applied at the top of the beam, equal to 1 if the load is applied at the bottom. However, the authors observed a significant underestimation of the experimental data. In fact, they remarked that this method considers the concrete contribution only in terms of stiffness, not strength, as explained in Eq. (27). Therefore, this method offers the benefit of providing practical formulations for engineers, since it simplifies the calculation of shear capacity as the number of yielded bars increases, but, as expected, it leads to conservative values of the shear capacity, the ratio between analytical prediction and experimental value being averagely equal to 42%.

The last experimental campaign reported here was conducted by Colajanni et al. [55] on two series of specimens, series A and B, tested under positive and negative three-point bending tests, respectively. The geometry of the samples is reported in Fig. 18.

The specimens had a cross-section of 300×250 mm in order to reproduce the behaviour of a slab-thick beam. The bottom chord of the truss was made with a 300×5 mm smooth steel plate (class S355), while the top chord of the prefabricated basic truss was constituted by three 16 mm rebars. Moreover, in all specimens, four rebars of the same diameter were added as top reinforcement. In specimens A2–1 and A2–2, two rebars with the same diameter were also added to the steel plate

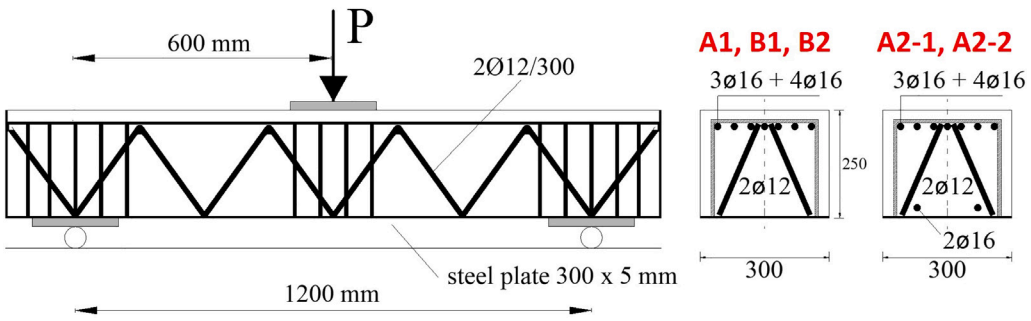

Fig. 18. Specimens tested by Colajanni et al. [55].

Table 5
Test results obtained by Colajanni et al. [55].

Specimen ID	A1	A2–1	A2–2	B1	B2
$P_u[kN]$	578	422	461	520	336
Concrete type	1	2	2	1	2

as bottom reinforcement. The basic truss was made with reverse V-shaped rebars with a diameter of 12 mm and spacing 300 mm. The steel grade of all rebars was B450C (i.e. ribbed steel); two concrete mixtures were created, namely concrete type 1 and type 2, with average compressive strength of about 25 N/mm^2 and 16 N/mm^2, respectively. The maximum loads obtained for all specimens are reported in Table 5. Among the specimens referred to in the table, specimens B1 and B2 were tested under negative bending moment, i.e. with the steel plate in compression.

The test outcomes showed that specimen A1 exhibited a shear collapse, with the initial formation of vertical cracks under the loading point, and the subsequent development of classical diagonal shear cracks. As in Chisari and Amadio [39], the specimen exhibited an overall ductile failure until the progress of the main diagonal shear crack, which caused a brittle shear failure. Conversely, samples A2–1 and A2–2, cast with the weaker concrete, exhibited from the beginning an evident brittle shear failure characterised by a partial detachment of the bottom steel plate from the concrete core. In general, the failure of the specimens was caused by the crushing of the compressed concrete strut. Specimen B1, cast with the stronger concrete and tested under negative bending moment, performed according to a mixed flexure-shear collapse mechanism characterised by a quasi-ductile behaviour. Conversely, specimen B2, cast with weaker concrete, exhibited a shear collapse failure characterised by a more brittle behaviour. None of the welds, whether between the steel plate and web bar or between the web and top chord rebar, showed any sign of damage.

An analytical model for the interpretation of these results was proposed by Campione et al. [49] who considered the combined resistance provided by concrete and shear reinforcement, assuming that the diagonal rebars of the steel truss function as transverse inclined stirrups, transferring stresses from the concrete to the bottom steel plate. The model also included the contribution of the diagonal rebars in both the shear force direction and the longitudinal traction direction, while also considering the contribution of the steel plate in the latter direction. The concrete contribution, V_{Rc} was computed as the capacity given by the sum of two resisting mechanisms, i.e. the arch effect, V_{Rc1}, and the beam action, V_{Rc2}, according to the following equations:

$$V_{Rc1} = \frac{j_0 d}{a}\left[\min\left\{A_b f_{yb}; q_{res,b}\cdot a\cdot\pi\sum_{i=1}^{n_b} D_i\right\} + \min\left\{A_p f_{yp}; q_{res,p} b_w^* a + \sum_{i=1}^{n_w} T_{wi} u(x-\bar{x}_i)\right\}\right] \quad (29)$$

$$V_{Rc2} = j_o d\left(q_{res,b}\pi\sum_{i=1}^{n_b} D_i + q_{res,p} b_w^* + \sum_{i=1}^{n(x)} T_{wi}\delta(x-\bar{x}_i)\right) \quad (30)$$

The symbols introduced in Eqs. (29) and (30) represent: $j_o d$, the inner lever arm; A_b, f_{yb} and D_i, the area, yielding strength and equivalent diameter of the longitudinal steel rebars; A_p, f_{yp} and b_w^*, the area, yielding strength and effective width of the steel plate; $q_{res,b}$ and $q_{res,p}$, the residual bond stresses around the longitudinal rebars and on the plate, respectively; T_{wi}, the dowel force attributed to each diagonal of the steel truss, whose calculation is reported in detail in [49]. Campione et al. [49] also assumed a limitation to the shear capacity of concrete given by the failure of the compressed concrete strut:

$$V_{Rc} \le V_{cu} = \nu f_c b\cdot x_c\cdot\frac{\sin(2\theta)}{2} \quad (31)$$

with ν a softening coefficient, θ the slope of the concrete strut and x_c the neutral axis depth.

In the proposed model, the contribution was assessed as:

$$V_{Rs} = A_{sw} f_{yw}\sin\alpha\sin\beta \quad (32)$$

assuming that α and β represent the inclination of the diagonals along the beam axis and in the cross-section plane, respectively. Therefore, the total shear capacity was given by the following expression:

$$V_R = V_{Rc} + V_{Rs} = \left(V_{Rc1} + V_{Rc2}\right) + V_{Rs} \quad (33)$$

with $V_{Rc} \le V_{cu}$.

In Campione et al. [49], this model was validated against the experimental tests previously described [55], obtaining a good agreement: the average ratio between analytical prediction and experimental shear capacity was about 0.97, with a coefficient of variation of 0.109. In the same study, the model was also validated against the test results obtained by Chisari and Amadio [39], and the ratio between theoretical and experimental shear capacity was an average of 0.92, with a coefficient of variation of 0.101, demonstrating a good agreement also in this case.

5. Beam-to-column joints

This section presents some relevant investigations conducted in the literature on the cyclic behaviour of beam-to-column joints with HSTCBs connected either to classical RC columns cast in place or hybrid columns equipped with internal reinforcement layout identical to that of the reference specimens, eventually encased in a steel tube profile [26,32,50,72,82]. The items of interest investigated in relation to the behaviour of joints are illustrated in the map of Fig. 19. The map shows that, in most cases, the analysed joints are made with HSTCBs with space double trusses and bottom steel plate; the research is mainly conducted through experimental tests, but analytical and numerical interpretations are also available. The mechanical performance of these joints is also investigated with regard to the seismic design of buildings according to the most recent strategies based on the energy dissipation capacity of structural components [64,68,70,75,78].

Therefore, in the following, two main items will be treated, i.e., firstly, the behaviour of traditional joints with HSTCBs and RC or composite columns and, secondly, the innovative design of connections in which the hybrid joint is integrated with dissipative systems.

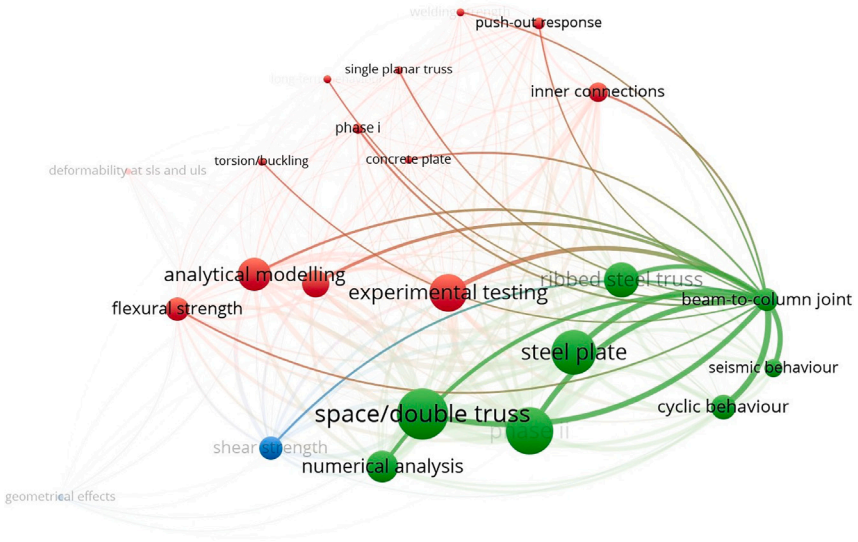

Fig. 19. Map of the keywords with higher co-occurrence with "Beam-to-column joint". (Created with VOSviewer [106]).

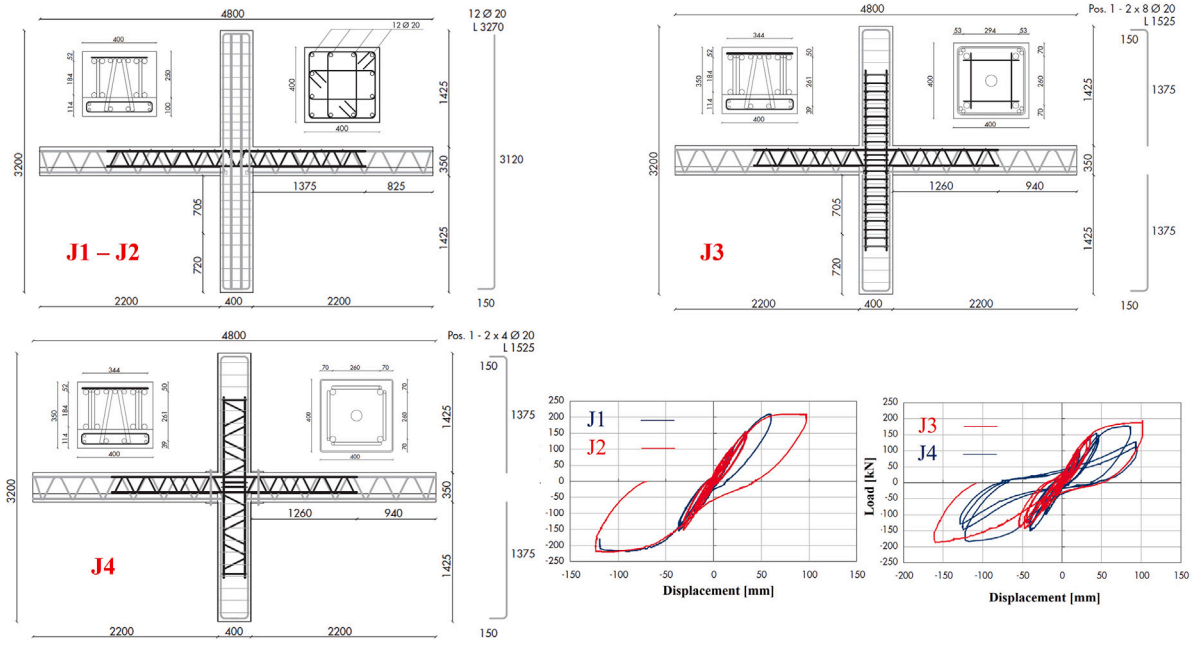

Fig. 20. Specimens of the joints tested by Scotta and Tesser [32] (dimensions in mm).
Source: Redrawn from [32].

5.1. Traditional joints with HSTCBs and RC or composite columns

The first experimental tests on hybrid joints considered in this section were performed by Scotta and Tesser [32] who tested five specimens, i.e. one reference classical RC joint (here referred to as J0); two joints with hybrid trussed beams and classical RC column (here referred to as J1, J2); one joint with HSTBs, RC column and cross-shaped integrated lattice (here referred to as J3); one joint with HSTCBs and RC columns jacketed with a cross-shaped integrated lattice (here referred to as J4). The details of the hybrid specimens are reported in Fig. 20.

In all cases, the HSTCBs utilised are made with a bottom concrete base and a space steel truss. The steel grade is S355 for both the base joist and the cross-shaped integrated lattice. The concrete compressive strength varied from 41 to 60 N/mm^2. The tests were conducted by supporting the two lateral ends of the beam (vertical displacements forbidden) and the bottom section of the column (horizontal displacements not allowed), while the lateral force was cyclically applied on the top of the column, in force control (±50 kN, ±100 kN, ±150 kN). Analysing the results, the authors found that the hybrid beam–column joints have demonstrated an experimental strength equal to the theoretical expectations, confirming the reliability of the structural system. These nodes also exhibited a larger ductility compared to the reference RC joint and achieved a maximum lateral displacement corresponding to an inter-storey drift of 4%. Finally, they observed that specimen J4, i.e. the joint equipped with the cross-shaped integrated lattice and jacketed column, exhibited the most limited damage of the panel zone compared to the other specimens. The load–displacement curves are reported in Fig. 20.

The second experimental investigation here summarised was performed by Amadio et al. [26] on one specimen of beam–column joint made with RC-encased steel joists. The column was 3.8 m in height,

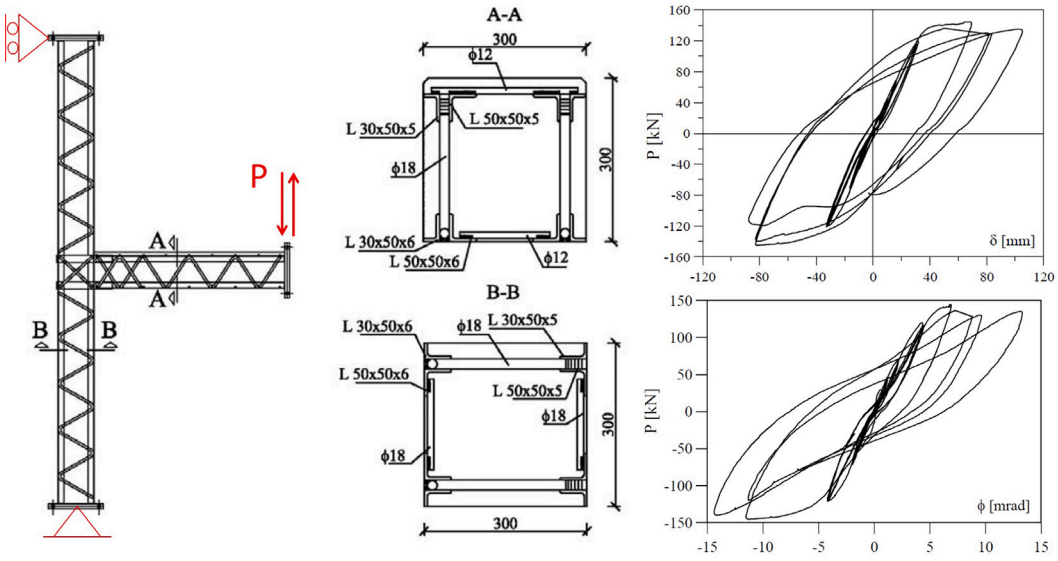

Fig. 21. Specimens of the joints tested by Amadio et al. [26] (dimensions in mm).
Source: Redrawn from [21,26].

simply supported at the two ends, and connected to a 2 m long cantilever beam, which was loaded at the free tip by a vertical force. A loading history in displacement control was applied, with cycles with amplitude up to +80 mm and -120 mm. Fig. 21 reports the details of the specimen, the loading scheme and the resulting load–displacement and load-rotation curves.

The collapse of the specimen occurred under a load of 145 kN. The failure happened in the beam at the point of the change in longitudinal reinforcement near the joint (at the end of the joint connecting plates), where there was a sudden reduction in cross-section and transverse reinforcement. At this load value, a significant shear crack propagated through the entire height of the beam, leading to the rupture of a longitudinal angle in the lower region, along with the crushing and expulsion of concrete in the upper region. The joint was also affected by significant diagonal cracking. The overall response in terms of load-rotation and load-end deflection showed that the energy dissipation capacity was high despite the premature collapse due to the shear cracking of the beam.

The authors also proposed an analytical interpretation of the shear capacity of the joint in compliance with Eurocode 2 [111], through the following equations:

$$V_{Rd,j} = V_{Rj,steel} + V_{Rj,conc} \tag{34}$$

$$V_{Rj,steel} = n_{diag} A_d f_{yd} \cos\alpha \tag{35}$$

$$V_{Rj,conc} = C \frac{0.25 f_{ck}}{\gamma_c} b_j h_j \tag{36}$$

In the equations above, the terms $V_{Rj,steel}$ and $V_{Rj,conc}$ represent the contributions to the shear capacity given by the diagonal steel bars and the concrete strut, respectively; C is a coefficient equal to 20 for external beam–column joints; b_j and h_j are the beam width and depth, respectively; n_{diag} is the number of diagonals in the joint and α their inclination with respect to the horizontal direction.

The authors calculated the theoretical shear capacity through Eq. (34), Eq. (35) and (36) finding that $V_{Rj,steel}$ = 314 kN, $V_{Rj,conc}$ = 450 kN and $V_{Rd,j}$ = 764 kN. The latter was compared to the experimental value, which was V_u = 670 kN, obtaining an overestimation of the predicted shear resistance. However, they also noted that the experimental failure of the joint was achieved prematurely at the failure of the beam, which was actually designed to resist bending and shear forces lower than the capacity of the joint.

The further experimental tests discussed here were conducted by Colajanni et al. [50] on three specimens of four-way joints made with HSTCBs and classical RC columns. It should be mentioned that previously, Colajanni et al. [44] tested three specimens of two-span continuous beams under monotonic and cyclic actions as a three-point bending test with the goal of investigating the behaviour of the end zone of the beam integrated into a moment resisting frame. However, such a loading scheme did not reproduce the seismic behaviour of the joint, and therefore, for brevity, it is not discussed in this section. In the test campaign reported hereafter from [50], the HSTCB was made up of a metallic spatial truss obtained with inclined steel bars for RC structures type B450C, as transverse reinforcement of the beam; these web bars were then connected superiorly to an upper chord constituted by coupled rebars of the same type of the truss through fillet weldings, and inferiorly butt-welded to a metal plate of smooth steel type S355. When preparing the joint specimen, four rebars with diameter of 24 mm where added as top reinforcement and two rebars with the same diameter on the bottom; all added rebars were passing through the panel zone. Conversely, the steel truss and its plate were stopped few centimeters before the joint because the truss was not equipped with bearing devices and, as a consequence, it did not exploit the self-bearing capacity. The average concrete compressive strength was about 37 N/mm^2. The test set-up was designed in order to apply a precompression to the specimens (800 kN in Test 1 and Test 2, 400 kN in Test 3), to simply support the beams at both ends and to finally apply the lateral cyclic load to the column base, the head being constrained through a hinge. Moreover, in the first test, the specimen was disposed with the steel plate of the beam on the bottom, while in tests n. 2 and 3, the specimen was collocated with the steel plate on the top. The details of the specimens and the load–displacement curves are reported in Fig. 22.

The results of Test 1 showed a maximum load of 128 kN for the joint, with a maximum drift of almost 8% at the end of the test. The crack of the panel zone started at about the fourth cycle, i.e. at about mid-test, and the plastic hinge at the end of the beam, next to the column face, was clearly visible at the end of the loading phases. From the stain gauge measurements, the authors also observed that the bottom plate near the joint, in the absence of sufficient anchorage, did not significantly contribute to the resistance of the joint, while increasing strain values in the plate were detected a little bit far from the joint, i.e. for reduced values of the bending moment, showing the efficacy of the diagonal rebars in transferring the stresses through the

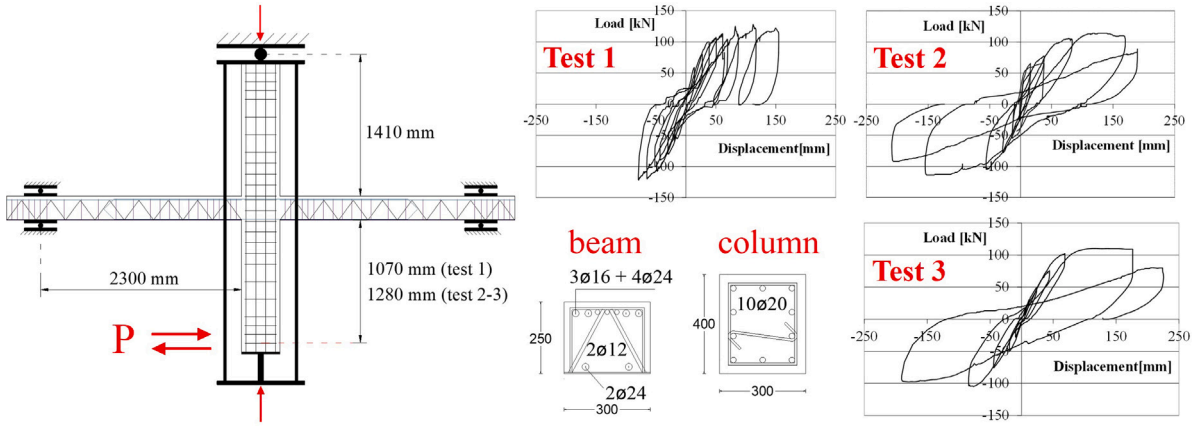

Fig. 22. Specimens of the joints tested by Colajanni et al. [50].

steel plate. In Test 2, the joint exhibited a maximum capacity of 112 kN and a larger maximum drift, of more than 10%. At mid-test, the crack of the panel zone was still limited, showing an increasing crack pattern starting from the fifth cycle, when the specimen exhibited relevant plastic displacements with a further increase of its load capacity. During the last cycle, the joint showed a significant pinching but still presented a residual strength of more than 70% than the maximum value. The last specimen exhibited behaviour similar to the previous one in terms of load capacity, crack pattern and reduction in stiffness and energy dissipation capacity during unloading and reloading cycles, but it achieved a slightly lower drift, equal to 7.6%.

For the analytical interpretation of the results, the authors in [50] considered two literature models, namely HL model (from Hwang and Lee [113]) and KLS model (from Kim et al. [114]). According to HL model [113], which is based on a strut-and-tie mechanism, the following equation should be written:

$$V_v = C_d sin\theta \tag{37}$$

$$V_h = C_d cos\theta \tag{38}$$

$$V_v/V_h = l_v/l_h = tan\theta \tag{39}$$

where V_v and V_h are the vertical and horizontal shear forces, respectively, while C_d is the diagonal compression, which has an inclination of θ with respect to the horizontal axis. The terms l_h and l_v represent the inner lever arm of the vertical and horizontal shear couples. Then, C_d can be calculated as follows:

$$C_d = -D + F_h/cos\theta + F_v/sin\theta \tag{40}$$

with D the compression force in the strut and F_h and F_v the tension forces in the horizontal and vertical ties, respectively. The system was statically indeterminate, so compatibility equations and material constitutive laws were required to determine the shear strength of the joint. Due to the nonlinear behaviour of the material, an iterative process was necessary to obtain the numerical solution.

According to KLS model, which is purely empirical, the following regression equation should be written:

$$V_{jh} = [\alpha_t \beta_t \eta_t \lambda_t (JI)^{0.15} (BI)^{0.30} (f_c)^{0.75}] b_j h_c \tag{41}$$

The parameters in Eq. (41) refer to the in-plane geometry (α_t), the out-of-plane geometry (β_t), the beam eccentricity (η_t); then $\lambda_t = 1.31$ for setting to 1.0 the overall average of the ratios of Eq. (41). Finally, BI is the beam reinforcement index, which depends on the beam reinforcement ratio and the volumetric transversal reinforcement ratio of the joint.

According to HL model, the authors assessed the shear capacity of the joint as 1115 kN for Test 1 and Test 2 and 903 kN for Test 3; similarly, according to KLS model, they assessed the joint shear capacity as 914 for Test 1 and Test 2 and 640 kN for Test 3 [50]. Then, they evaluated the experimental shear resistance through the following equation:

$$V_{jh,exp} = 1.2(A'_s + A_s) f_y - V_{c,exp} \tag{42}$$

with, A'_s and A_s the area of the top and bottom rebars having a yielding strength of f_y, and $V_{c,exp}$ the ultimate load applied to the specimen. From Eq. (42) it resulted $V_{jh,exp} = 1501$ kN for specimens 1 and 2, while $V_{jh,exp} = 978$ kN. Therefore, if compared to the analytical prediction, the average ratio between experimental and theoretical shear capacity considering the HL model was equal to 1.27, while it resulted in 1.61 if KLS model was considered. In both cases, the predictions gave a conservative result.

More recently, Albright et al. [72] developed an experimental campaign on exterior and interior joints made with HSTCBs and RC columns. They tested nine specimens, two of which were RC reference samples. In the hybrid joints, the beam was equipped with a bottom steel plate (5 mm×400 mm), two planar parallel trusses made of smooth steel with four upper 26 mm plain bars and diagonal bars with 20 mm of diameter and 400 mm spacing, welded to the bottom plate. Additional reinforcement was added to the beam by 30 mm rebars to the top and bottom, making the joint continuity. Among all specimens, the one labelled NPS1 was equipped with two additional inner trusses, planar and parallel to each other, identical to the basic trusses but located in the inner core of the cross-section of the beam, making the joint continuity. The column was made of reinforced concrete, with a cross-section of 400×400 mm and 12 rebars of diameter 28 mm, finally encased in a steel tube. The material properties were concrete compressive strength of 40 N/mm^2 and yielding strength of steel equal to 450 N/mm^2. Fig. 23 shows the details of the specimens and the test set-up, together with the cyclic load–displacement curves of the relevant typologies of joints.

The authors in [72] observed that all systems achieved their targeted design strength and demonstrated good ductility. Generally, interior joints experienced joint failure following beam yielding at the beam–column interface, whereas exterior joints did not show signs of distress in the joint and experienced beam yield failure. In both scenarios, the system's demand was governed by the yield strength provided by the continuity elements at the beam–column interface. All interior joints exhibited a pinched force–displacement behaviour due to bond–slip deterioration caused by the high bond demand on the continuity bars. Despite the observed pinching, almost all systems demonstrated satisfactory levels of strength, ductility, stiffness, and energy dissipation. Finally, they observed that all exterior joints exhibited excellent performance, without deterioration of the panel zone and only minimal bond–slip deterioration. Their force–displacement

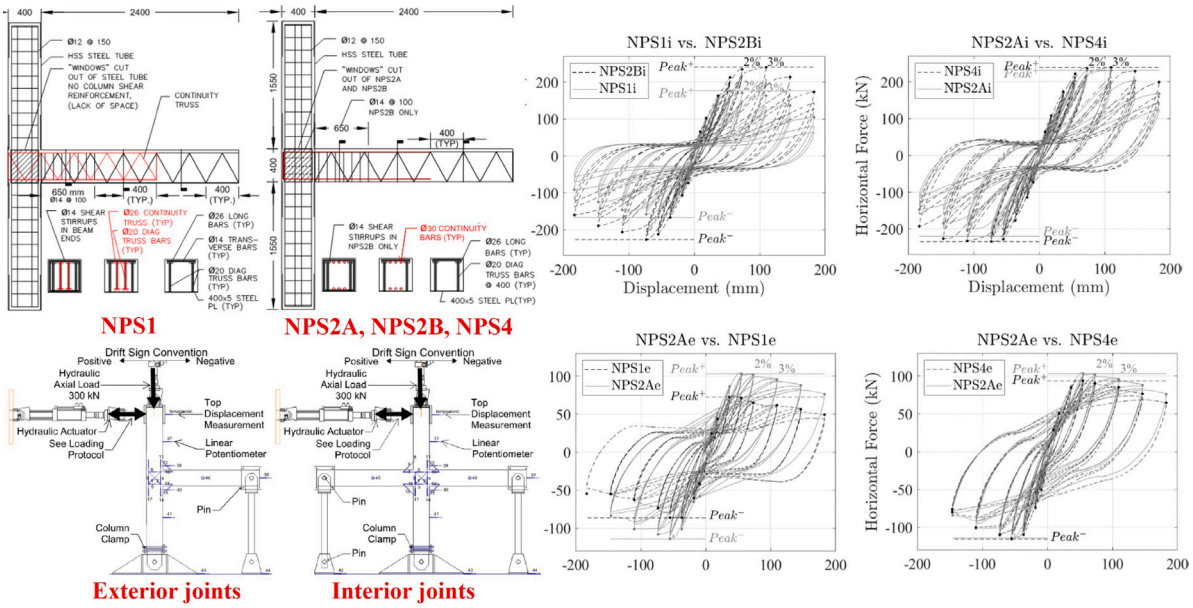

Fig. 23. Specimens of the joints tested by Albright et al. [72] (dimensions in mm).
Source: Redrawn from [72].

response was characterised by large hysteretic loops, indicating high energy dissipation and ductility levels.

The last experimental program here considered was very recently conducted by Di Cesare et al. [82] on two specimens of steel-trussed concrete beam ductile joints, made with the same beam but two different columns, i.e. RC column in one specimen, and concrete-filled steel tube in the other specimen. In both cases, an exterior joint is considered, but two different constraints are assumed at the column base, namely a hinge for the specimen with an RC column (specimen 1) and a fixed restraint for the specimen with the concrete-filled tube column (specimen 2). Both specimens are equipped with the same composite precast truss beam, whose cross-section is 300×250 mm; the steel truss ended before the column, and the two end parts of the beam consisted of a simple RC section reinforced with six 24 mm steel rebars anchored within the joint panel. Specimen 1 comprised concrete class C28/35, while specimen 2 had concrete class C40/50. For both specimens, reinforcement rebars and steel elements were made with steel grade B450C and S355, respectively. The loading scheme was characterised by a constant axial force of 80 kN applied to the column and a triangular load with a resultant equal to 34 kN applied to the beam. The scope of this scheme was to reproduce the loading and specimen deformation due to only gravitational loads. In the first stage of the test, the beam was free to deform, while in the second stage, a rigid rod was applied at the end of the beam in order to reproduce the deflection points; in this phase, the lateral load was finally applied on the top of the column. Quasi-static cyclic tests were conducted in displacement control by means of twelve consecutive tests, each one characterised by three cycles of displacements applied to the specimen. Fig. 24 reports the specimen details and the load-drift curves of the cyclic tests.

From the analysis of the test results, the authors in [82] found that the global behaviour of the two specimens was different because of the diversity of geometrical features, boundary conditions and concrete compressive strength. Nevertheless, the results also showed similar local performance in terms of the crack pattern detected at the end of the test in the panel zone. Moreover, in both specimens, the plastic hinge deformation was observed at the end section of the beam, starting from about 1% of drift; the plasticisation of the section was characterised by stable behaviour with a large amount of energy dissipation and a limited reduction in strength. In general, the cyclic curves revealed, in both cases, good dissipative and ductile capacities. Both joints were able to support gravity loads despite the relevant reduction of global stiffness and strength related to the damage developed after the first half of the loading history.

5.2. Dissipative connections in seismic areas

Recent studies have addressed the design of innovative connections in buildings in seismic areas to improve the dissipation capacity through the joints [83]. To achieve this goal, the latest design strategies adopted in steel-framed structures have been re-adapted to RC buildings equipped with HSTCBs (among the most relevant, [64,68,70,75]). The up-to-date contribution proposed by Monaco et al. [78] revealed the design process of a novel patented solution [115] of a hybrid beam–column connection equipped with friction-damping devices. The concept of this friction connection in the joint between the HSTCB and the RC column involved steel members that served as the rotation centre at the top of the connection; additionally, a system of three steel plates in contact through friction bolts was situated at the bottom of the connection. Consequently, both the top and bottom steel profiles were linked by special devices to the RC column and the hybrid beam, forming the friction-damping system. Three design solutions were proposed schematically depicted in Fig. 25.

The friction connection design process started with the value of the design bending moment, M_d, which triggers the system's slippage. The design procedure aimed to prevent device slippage at the serviceability limit state, while allowing energy dissipation through sliding during seismic events. Therefore, the device geometry was determined through an iterative process to find the optimal internal lever arm value, z_i, for each proposed solution (where $i = 1, 2, 3$ for solutions A, B, and C, respectively). The, in order to conduct a feasibility study, an arbitrary value of $M_d = 110$ kNm was assumed. This value was compatible with the hogging moment strength of the beam in the subassembly, $M_{Rd} = 165$ kNm, calculated with an overstrength factor of 1.5. Finally, the friction damper was designed to withstand a sliding force, $F_{d,i}$, determined as follows:

$$F_{d,i} = \frac{M_d}{z_i} \tag{43}$$

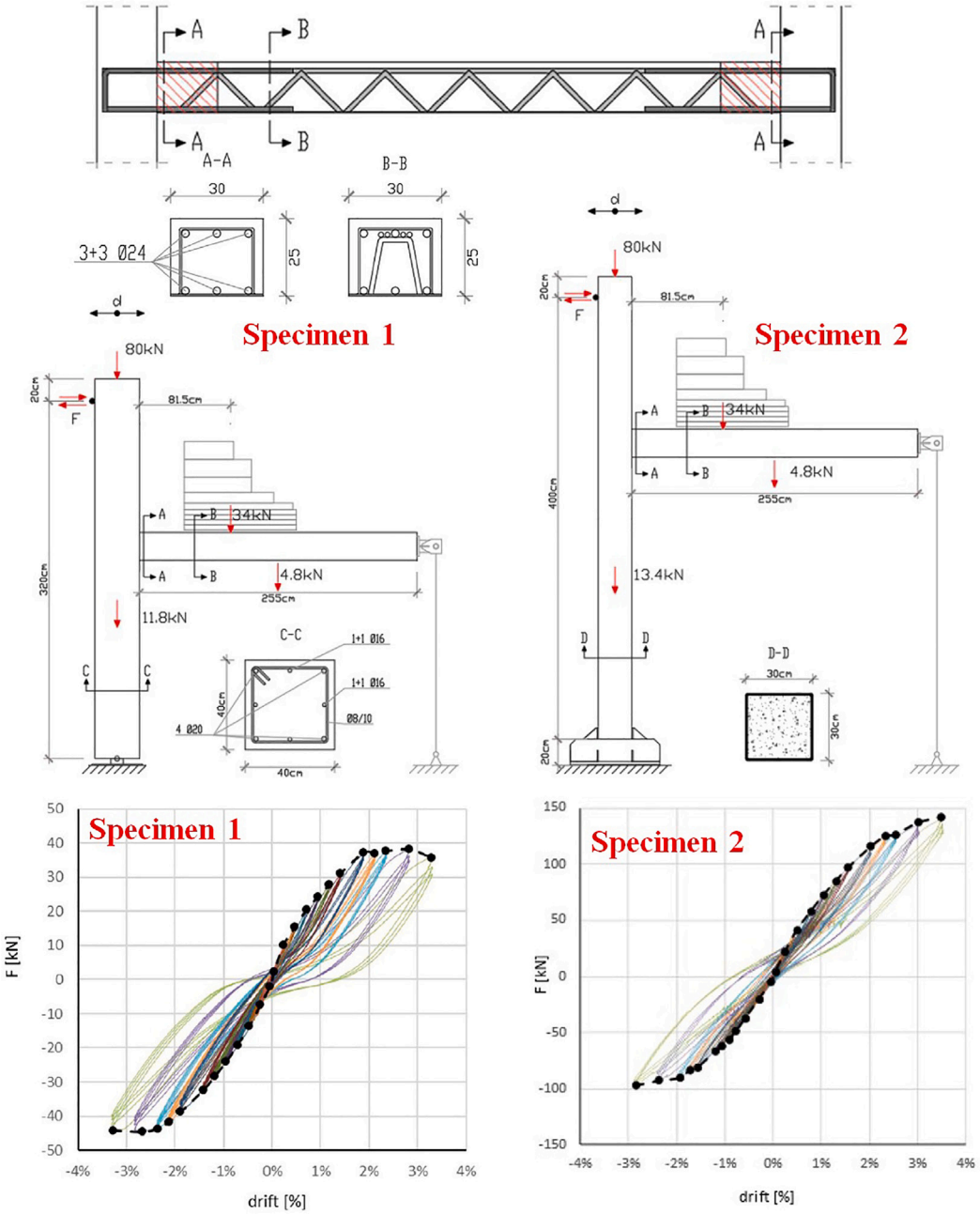

Fig. 24. Specimens of the joints tested by Di Cesare et al. [82].
Source: Redrawn from [82].

The number of preloaded bolts used was $n_{b,i}$ with an area $A_{res,i}$ and ultimate strength $f_{ub,i}$. The preloading force $F_{pc,i}$ of each bolt, as per Eurocode 3 [108], was calculated as follows:

$$F_{pc,i} = 0.7\, f_{ub,i} A_{res,i} \tag{44}$$

and the code-compliant slip resistance of the connection, $F_{s,Rd,i}$, was evaluated as:

$$F_{s,Rd,i} = k_s n_{b,i} n_s \mu F_{pc,i} / \gamma_{M3} \tag{45}$$

In Eq. (45), k_s and γ_{M3} are coefficients introduced in the design formula to prevent the device from sliding until the ultimate limit state (assumed equal to 1 in [78]). The terms n_s and μ represent the number of friction planes and the slip factor, respectively. For all proposed solutions, $n_s = 2$ and $\mu = 0.4$ were assumed [78].

Considering that the preload value decreases over time due to creep phenomena, the adopted design preloading force $F_{pc,d,i}$ was in the range between 30%–60% of the code-compliant value given in Eq. (44). The ratio between effective and code-compliant preload was assessed using the coefficient $t_{s,i}$:

$$t_{s,i} = \frac{F_{d,i}}{n_{b,i} n_s \mu F_{pc,i}} \tag{46}$$

Finally, the effective design value of preload was assumed equal to:

$$F_{pc,d,i} = t_{s,i} F_{pc,i} \tag{47}$$

The authors observed that according to Eq. (46), the parameter $t_{s,i}$ indicates the stress level of each preloaded bolt and, therefore, the design procedure allows for the diameter of the preloaded bolts to be adjusted to achieve the same preloading force at different stress levels [78]. Regarding the dimensions of the slotted holes, they were

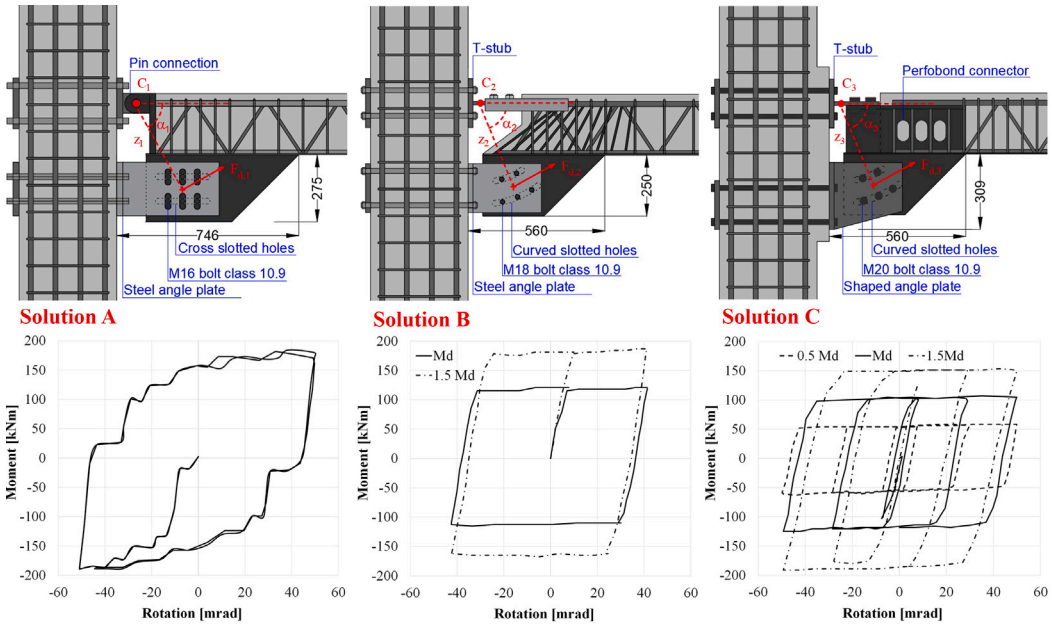

Fig. 25. Design solutions of dissipative connections (dimensions in mm) [78].

designed based on the displacement demand of the structure. Lastly, the steel members connected to the upper and lower parts of the beam and column were sized to withstand both the horizontal and vertical components of the design sliding force from Eq. (43), amplified by the overstrength factor.

The three proposed solutions were based on the same design criteria, but they differed in the arrangement of the components because Solution A was characterised by a friction device endowed with a hinged connection and crossed slotted holes, Solution B was a friction device equipped with a T-stub, curved slotted holes and shaped concrete section of the beam, while Solution C represented a friction device with shaped T-stub, curved slotted holes and perfobond connectors.

More in detail, in Solution A, the pin connection on the top made the rotation centre of the system, C_1, while the bottom connection was made with two lateral steel angles connected to a central plate using six M16 class 10.9 bolts with $A_{res,1} = 157$ mm^2 and $f_{ub,1} = 1000$ N/mm^2. The steel angles and the central plate had slotted holes in the vertical and horizontal directions. The cross-section of the beam measured 250 × 300 mm, with an inner lever arm $z_1 = 399$ mm. The angle between the beam axis and the sliding force's application point was $\alpha_1 = 61°$. In this configuration, $F_{d,1} = 275.7$ kN,$F_{pc,1} = 109.9$ kN, $t_{s,1} = 0.523$, and $F_{pc,d,1} = 57.5$ kN. The main disadvantage of this solution was the clearance around the pin of the hinged connection, which caused additional sliding and friction resistance before the activation of the designed mechanism, with the rotation centre C_1 not exactly centred in the pin since the beginning of the loading process.

In Solution B, five bolts were collocated along two rows of curved slotted holes, with the rotation centre C_2 determined on the weakest section of a T-stub placed on the top connection to replace the pin of the previous solution. This T-stub was then connected to the beam by means of a C-shaped steel profile. In this case, the preloaded bolts were M18 of class 10.9, with $A_{res,2} = 192$ mm^2 and $f_{ub,2} = 1000$ N/mm^2. The angle $\alpha_2 = 68°$ and the inner lever arm $z_2 = 380$ mm. Consequently, the authors found $F_{d,2} = 289.5$ kN, $F_{pc,2} = 134.4$ kN, $t_{s,2} = 0.538$, and $F_{pc,d,2} = 72.3$ kN. This solution was able to overcome the issues detected in the previous one even though it showed inadequate stiffness of the top bolted connection and still slight shifting of the rotation centre due to the plasticisation of the T-stub cross-section.

Therefore, the last Solution C was proposed with further improvements compared to the others. First of all, the authors here proposed an extension of the central curved-slotted plate throughout the beam, further equipping this extension with slotted holes useful to make a so-called perfobond connector. The vertical extension of the plate is then welded to a horizontal plate with slotted holes, on which the T-stub and the longitudinal top rebars of the beam are welded. Also in this case the T-stub was provided with a weakened section for the development of the plastic hinge (rotation centre C_3). In this system, two rows of curved slotted holes were designed, introducing five M20 class 10.9 bolts ($A_{res,3} = 245$ mm^2 and $f_{ub,3} = 1000$ N/mm^2). The inner lever arm was $z_3 = 374$ mm and the angle $\alpha_2 = 68°$. Therefore, the following parameters were found: $F_{d,3} = 294.12$ kN, $F_{pc,3} = 171.5$ kN, $t_{s,3} = 0.429$, and $Fpc,d,3 = 73.5$ kN. The main advantage of this solution was the additional shear strength developed thanks to the dowel action provided by the perfobond connector system and a more stable behaviour.

The structural performance of the three proposals was investigated through the numerical simulation of a cyclic loading scheme on the joint specimens. Fig. 25 shows the comparison between the moment–rotation curves obtained through FEM analyses. The cyclic analysis of the first joint (Solution A) was conducted in the range of ±100mm. The simulated behaviour of the joint showed the negative effect of the clearance around the pin connection, which was notable due to the presence of two sub-horizontal branches in the curves. These branches signified the resistance the friction plates offered when the pin initially moved inside the hole before establishing contact. This behaviour significantly impacted both the stiffness of the system and its ability to dissipate energy effectively.

The cycles applied to the joint of Solution B were too in the range of ±100mm. Additionally, analyses with varying preload levels in the bolts were conducted to simulate the system's behaviour under two different design moment values: M_d and $1.5M_d$, with 1.5 the overstrength factor. The simulation results indicated that the system adhered to the design assumptions, with a similar response observed for positive and negative bending moments and no significant damage was observed during the loading-unloading phases. However, after an initial elastic phase with no sliding, an almost perfectly plastic branch emerged when sliding was initiated, and the upper T-stub underwent plasticisation, resulting in a slight displacement of the designed rotation centre.

Finally, the simulations of the third joint (Solution C) were made for three values of the design bending moment, namely $0.5M_d$, M_d,

and $1.5M_d$. The results of the analyses indicated that this connection had sufficient stiffness to prevent any shifting of the system's centre of rotation. The hysteresis loops were wide and stable, meeting the design requirements, and the system's response varied proportionally with changes in the bolt preload.

In conclusion, the initial Solution A with a pin connection exhibited a pinching effect in its cyclic response due to clearance in the pin connection and additional resistance from the dissipative device caused by bolt shifting during sliding, primarily through vertical and horizontal translations. Consequently, Solution B addressed these issues by replacing the pin connection with a bolted configuration involving a T-stub and C-shaped profile and implementing curved slotted holes in the friction plates instead of crossed slotted holes. Even though Solution B exhibited improved performance, it revealed weaknesses such as inadequate stiffness in the top bolted connection, contributing to the centre of rotation shifting during analysis. Therefore, the third proposed solution, Solution C, introduced perfobond connectors and a reduced T-stub middle cross-section, resembling the steel structures' dog-bone-shaped beam ends. Solution C effectively resolved the remaining weaknesses of Solution B and ensured minimal damage to all components within the connection device; therefore, the authors stated that it represents a promising damping system for semi-prefabricated RC buildings equipped with HSTCBs [78].

6. Open issues

Following a thorough synthesis of the primary findings described in the previous sections, the literature review highlights significant gaps in knowledge and unresolved issues, particularly regarding long-term performance and geometrical effects.

6.1. Long-term performance

Concerning, long-term behaviour, the literature only reports the experimental and numerical analyses conducted by Sassone and Casalegno [29], who studied two different configurations: a simply supported beam measuring 10 meters in length and having a cross-section of 300x350 mm, and a pair of beams of the same dimensions, connected by introducing a fixed constraint at a later stage at the intermediate support. Although this second scenario is more common in construction using precast concrete elements than HSTCBs, for the authors, it represented an important test for assessing the impact of viscosity on the redistribution of internal forces and deformation states. The first approach followed in [29] was a computational viscoelastic analysis conducted in the field of the General Method by coupling the traditional discrete solution procedure of integral equations with a FEM solver that provides specific simulation tools for the analysis of reinforced concrete structures. In particular, they assumed a beam with three different reinforcement ratios ρ equal to 1%, 5% and 10% and calculated the midspan deflection, f, in time, t, as shown in Fig. 26.

Two primary results emerged: on one hand, viscous deformations, assuming a fully reactive concrete section, were significantly influenced by the amount of reinforcement. For reinforcement ratios exceeding 5%, the delayed deformation was either smaller or equal to the initial deformation, whereas, with minimal reinforcement percentages, delayed deformations could reach up to twice those of the initial ones. Therefore, the contribution of reinforcement resulted in a substantial reduction in long-term delayed deformations. Moreover, the difference in prediction obtained by applying the various viscosity models proposed in the literature varied significantly. Between the European model CEB90 and the US models B3 and GL2000, in particular, there was a substantial difference in prediction after approximately 1000 days: while the CEB90 model assumed an asymptotic trend, suggesting a substantial settling of the phenomenon, the other two models, albeit differently, predicted instead a continuation of the phenomenon even over timescales of one or two orders of magnitude longer. When the later constraint was introduced, a discontinuity clearly emerged with a subsequent reduction of the long-term deformation. These numerical investigations showed that HSTCBs exhibited particularly good long-term performance. Therefore, experimental tests were performed as validation tools to achieve more accurate results. Four samples of simply supported beams were constructed, using the HSTCB type with lower steel plate, and two further beams with similar general characteristics but equipped with bottom concrete base. In all specimens, the rebars were made only of ribbed steel. The beams were designed to produce an initial deflection of approximately 20 mm under the applied load. The main challenge in these tests was the application of long-duration loading, which was addressed by using steel sheet packages corresponding to a load of approximately 4.00 kN/m. Given the relatively modest load, the beams were designed to be particularly slender, with a nominal cross-section of 190x200 mm for the beams with steel plate and 200x240 mm for the beams with concrete base. The specimens had a total length of 5960 mm; the spacing between diagonals was 340 mm and 360 mm for steel plate and concrete base beams, respectively. Moreover, the beams were designed with different reinforcement ratios, reaching a maximum value of approximately 9%. Fig. 27 reports the structural details and the long-term deflection of two beams taken as an example, namely beam n. 101 (with steel plate) and beam n. 105 (with concrete base).

The experimental deflection was manually measured in a discrete way, at day number 14, 15, 17, 20, 27, 45, 56, 63, 91 and 144. Then, the experimental data were compared with the numerical predictions as shown in the graphs of Fig. 27. The authors found that, over the considered time frame, the long-term deformations due to viscous phenomena measured experimentally were in good agreement with the numerical predictions. The largest discrepancies concerned the magnitude of the initial deformations, which were influenced by imperfections in the testing apparatus. The presence of high reinforcement ratios, which was explicitly considered in the simulations, had a beneficial effect in reducing viscous deformations, and this effect was predicted with a good level of reliability. Even though this study provided promising results, further tests would be useful for validation, and additional numerical studies should be conducted to analyse the effects of the bottom chord of the beam (steel plate rather than concrete base, with or without additional longitudinal reinforcement) on the long-term deflection in the serviceability limit state. Finally, the influence of the geometrical layout of the steel truss should be investigated, aiming at optimising the beam design.

6.2. Geometrical and size effects

The second open issue considered in this section is related to the investigation of the geometrical effects on the mechanical performance of the HSTCB, including the analysis of the size effect. First of all, it is noteworthy to mention two scaling transition laws from the literature, which are the Size Effect Law (SEL) [116] and the Multi-Fractal Scaling Law (MFSL) [117], the first one based on dimensional analysis, the second one funded on fractal geometry. SEL is valid for initially cracked specimens, the initial crack length being proportional to the specimen size, while MFSL is based on Renormalization Group Theory and is valid for initially uncracked specimens. In this regard, the concept of size effect on single material strength and the issue of scale effect on structural brittleness should be distinguished and analysed. In fact, especially in cases where particularly large or particularly small structures are involved, the strength of the material must be compared against other characteristics, such as the toughness in the case of fracturing processes, in order to define, via the structural size, the ductility or the brittleness of the structure [118–120].

A very limited number of studies in the literature aimed at addressing the topic of geometrical effects on HSTCBs. A recent study was conducted by Etman et al. [89] on RC beams reinforced with internal trussed strips and bars placed in the shear span zone. In this study, the

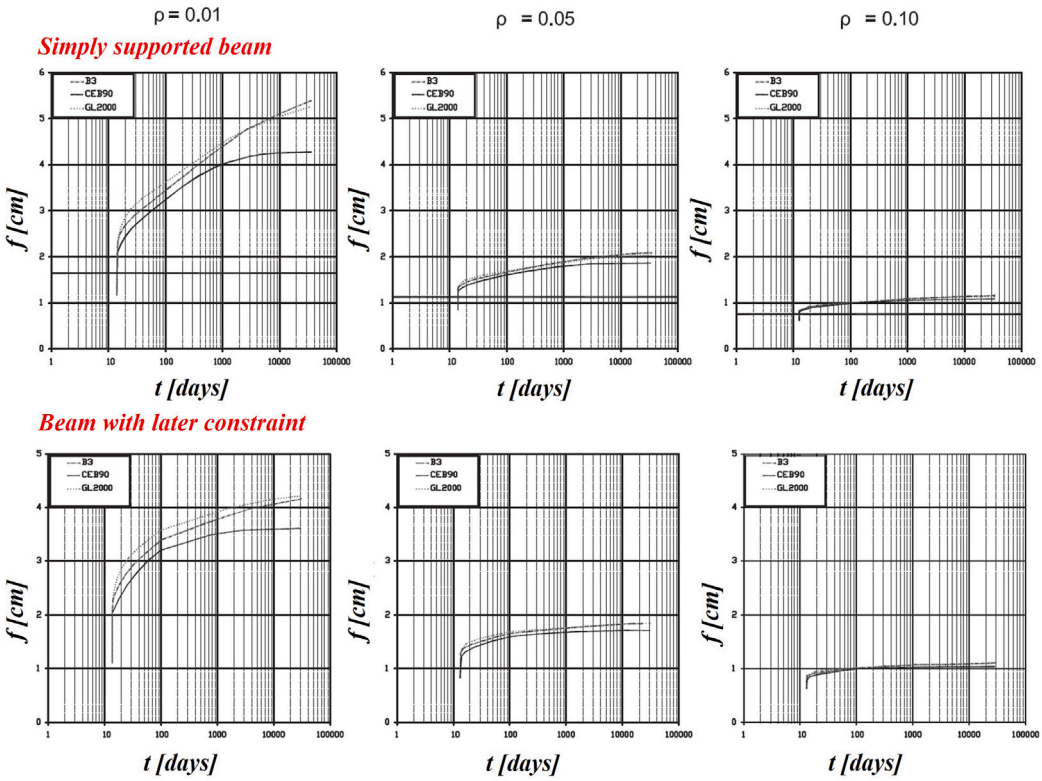

Fig. 26. Numerical long-term mid-deflection of the beams tested by Sassone and Casalegno [29].
Source: Redrawn from [29].

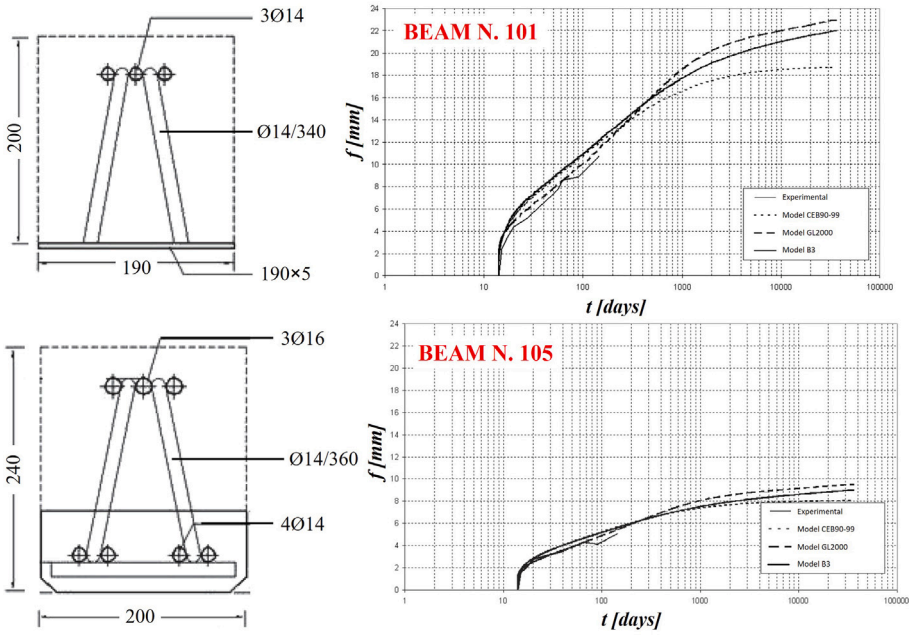

Fig. 27. Long-term deflection experimental tests by Sassone and Casalegno [29] (dimensions in mm).
Source: Redrawn from [29].

truss was characterised by two parallel systems of diagonal strips made of smooth steel. The hybrid beams were tested under four-point bending, assessing the structural performance of different reinforcement layouts, which varied for the strip configuration (vertical, inclined, and trussed strips with the same width of 25 mm and the same spacing of 200 mm), the strip cross-sectional areas (trussed strips of 14 mm and 40 mm width, with the same spacing of 200 mm), and the strip spacing (160 mm and 265 mm, with the same cross-sectional width of the trussed strips equal to 25 mm). Similarly, different layouts were also tested in the case of inclined and trussed bars: vertical, inclined, and trussed bars with the same diameter of 8 mm and the same spacing of 200 mm; trussed bars of diameter of 6 mm and 10 mm, with the same spacing of 200 mm; trussed bars with the same diameter of 8 mm and different spacing of 160 mm and 265 mm. Based on the experimental

results, the authors observed that the ultimate capacity of the beams reinforced with trusses was directly related to the cross-sectional area of the truss members and inversely related to the spacing between the vertical members. Nonetheless, the ultimate capacities of beams reinforced with trussed strips exceeded those of beams reinforced with equivalent trusses made from rounded bars of about 16%. Moreover, they also observed that considering the cross-sectional area of the truss members and the spacing in the tested different configurations, the shear crack width at any load level was smaller in beams reinforced with trussed strips compared to the corresponding beams reinforced with equivalent trussed bars. Finally, the authors in [89] also mentioned a gap of knowledge in the literature concerning the lack of an analytical expression for calculating the load value which corresponds to the maximum shear crack width. This topic is not fully defined in the literature, leading to some discrepancies between the experimental results of major shear crack width and the analytical results derived from existing models. In their research, the authors found that, despite the differing load levels as a percentage of failure load corresponding to the measured shear crack width, the experimental results were comparable to the results from some available equations proposed for calculating shear crack width. However, a new reduction factor should be introduced in order to account for the type of reinforcement, whether single or trussed steel strips.

The effects of different layouts of steel trusses were also numerically analysed in a study conducted by Taher et al. [91], who considered five specimens with the same overall dimensions and longitudinal reinforcement equipped with different steel trusses. However, the major limit of this study is the focus on the solely geometrical spacing of the truss, considering the presence or the absence of added vertical bars. Therefore, the main finding was limited to the evidence that the adoption of embedded steel truss as web reinforcement resulted in an increased ultimate capacity of the beam of about 4%–8% compared to the control specimen, which was reinforced only with vertical stirrups.

Similar considerations can also be conducted regarding the recent analysis by Lofty et al. [92] on hybrid trussed beams adopted in aerospace shelters. Here, the authors simply considered two different configurations, i.e., beams with vertical strips and beams with inclined trussed strips, and two main layouts for the inclined strips, i.e., an inclination angle of 45° or 60°. Under these hypotheses, the authors found an improvement of the flexural capacity of about 11% in the trussed beams compared to the standard reinforced beam and a significant ductile behaviour in the post-elastic phase.

In conclusion, in the aforementioned studies, neither the issues related to size effect nor the influence of the geometrical layout in the transition between flexural and shear failure were investigated. Conversely, in this regard, the studies previously conducted by Ballarini et al. [53,65] should be mentioned. In these studies a computational analysis was proposed for detecting the different failure modes in HSTCBs with different scaled sizes chosen from considerations on some typical dimensions adopted in the industrial practice. Fig. 28 shows the beam specimens considered by Ballarini et al. [53,65]: they were characterised by three different scaled geometries labelled size 1, 2 and 3, with the same cross-sectional width (b = 300 mm), the same longitudinal reinforcement (upper chord made of seven rebars of diameter 16 mm and lower chord made of a 5 mm thick steel plate) and the same transversal reinforcement (steel truss with 12 mm reverse V-shaped rebars). The overall dimensions were established in order to keep the ratio between shear span a and beam depth D constant and equal to $a/D = 2.4$. Therefore, the horizontal span of the steel truss is linearly scaled with the beam depth, resulting in different slopes of the diagonals in the plane of the cross-section as well as along the longitudinal axis of the beam. Since the steel reinforcement of the beams was not scaled, the three specimens did not exhibit geometrical similarity, which consequently affected their failure modes. The latter were therefore investigated through FEM analyses by exploiting the validation against the experimental results obtained in separate research on the size 1-beam [55]. For conducting the analyses, the material properties assumed in all specimens were the same: compressive strength of concrete equal to 25 MPa, steel class B450C for the ribber rebars and steel class S355 for the bottom plate. First of all, a simplified model was developed in which a perfect bond was assumed between rebars and concrete, showing that it was satisfactory for catching the peak load capacity and the overall energy dissipation of the beam and computationally efficient, compared to more detailed modelling of the steel-concrete interface by means of cohesive contact laws. To this scope, the graphs in Fig. 28 show the comparison between the curves obtained with perfect bond and cohesive models. These curves also evidenced a transition from fragile and ductile failure passing from the smallest to the biggest size.

This result was explained analytically by adopting the approximate size and geometrical effect equation proposed by Bažant [116,121] for calculating the nominal structural strength σ_N:

$$\sigma_N = \sigma_0\left(1 + D/D_0\right)^{-1/2} \tag{48}$$

in which σ_0 is the nominal structural strength at the small-size limit while D_0 is the transitional size. Moreover, in [53,65] the nominal structural strength is calculated as:

$$\sigma_N = P_{max}/bD \tag{49}$$

in which P_{max} is the maximum load capacity of the beam, D is the characteristic size (i.e. the beam depth), and b is the beam width.

The shear failure observed in the smallest specimen followed the same mechanism as the diagonal shear failure in conventional RC beams. Consequently, Eq. (48) was expected to adequately approximate the size effect in the shear failure of HSTCBs, by describing the transition from quasi-plastic shear failure to brittle shear failure as the specimen size becomes much larger than the size of the fracture process zone. Therefore, if Eq. (48) represented the size effect for the diagonal shear failure mode, a different relationship was derived for the nominal structural strength achieved in the case of flexural failure. In particular, the authors neglected the concrete damage in the diagonal direction and assumed that only the yielded bottom steel plate contributed to the tensile response. Therefore, they calculated the bending moment capacity at the midspan as $M_u = f_y A_s \overline{d}$ (with f_y and A_s the yielding strength and cross-sectional area of the bottom plate, and $\overline{d}$ the effective depth of the beam) and the peak load as $P_u = 4F_y A_s \overline{d}/L$. Considering that the size of the beam was scaled in two dimensions, the ratio $\overline{d}/L$ was assumed constant. According to these assumptions, a parameter η was defined as $\eta = 4F_y A_s \overline{d}/bL$, and the corresponding scaling equation was written:

$$\sigma_N = \eta D^{-1} \tag{50}$$

Finally, the nominal structural strength of the beam was assessed as follows:

$$\sigma_N = \min\left[\eta D^{-1}, \sigma_0\left(1 + D/D_0\right)^{-1/2}\right] \tag{51}$$

Fig. 29 shows the schematic plot of Eqs. (48) and (50), evidencing how size 2 and size 3 specimens were aligned with the analytical prediction of the flexural failure mode, with the size effect derived by a simple plastic analysis. In contrast, size 1 specimen was expected to follow the analytical prediction of the shear failure mode, with the size effect described by using the classical Bažant's size effect law of quasi-brittle fracture.

This analysis identified a transition point between the two expected failure modes, which was influenced by the geometrical features of the bottom steel plate in the three specimens. In particular, the authors evidenced that the steel plate was not scaled in order to keep its thickness coherent with the dimensions adopted in the industrial practice. However, this assumption represented a mechanical disadvantage for the beams with the biggest size because, if the thickness of the steel plate were scaled proportionally with the beam size, the size effect on nominal strength in the flexural failure mode would disappear.

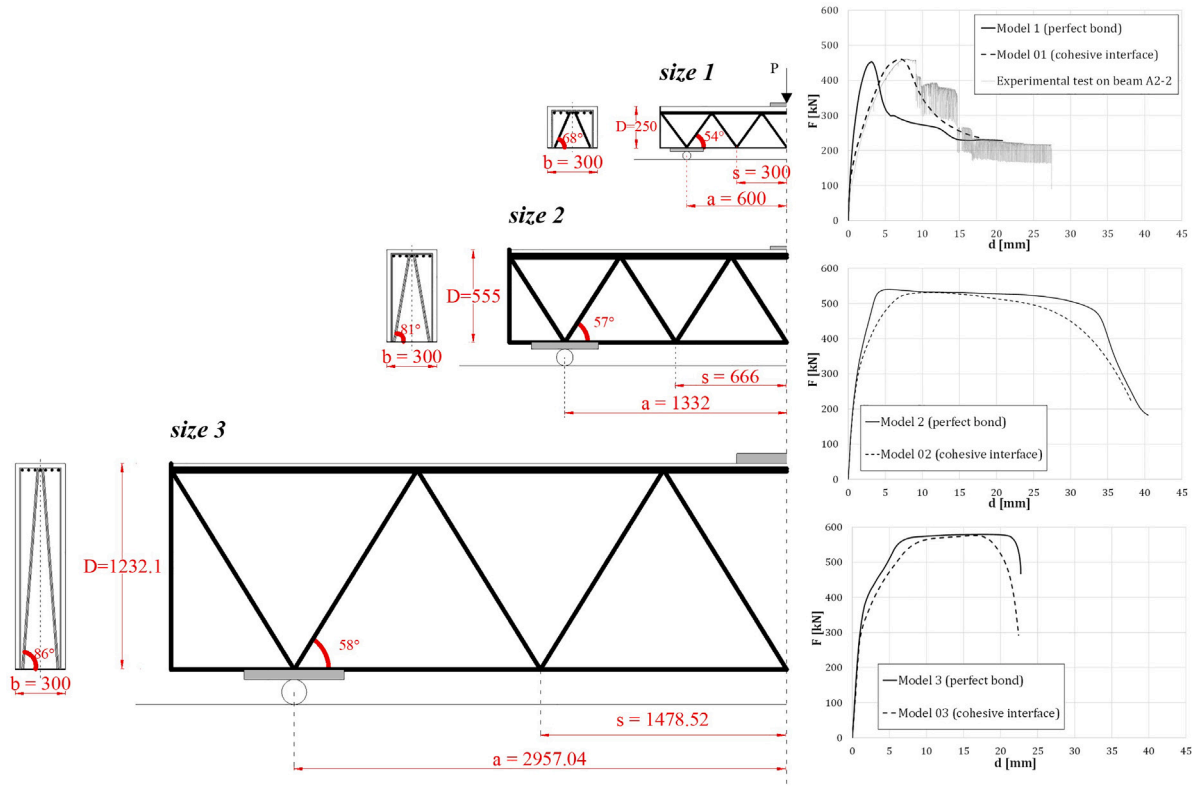

Fig. 28. Analysis of the geometrical effects on different beam sizes (dimensions in mm) [53,65].

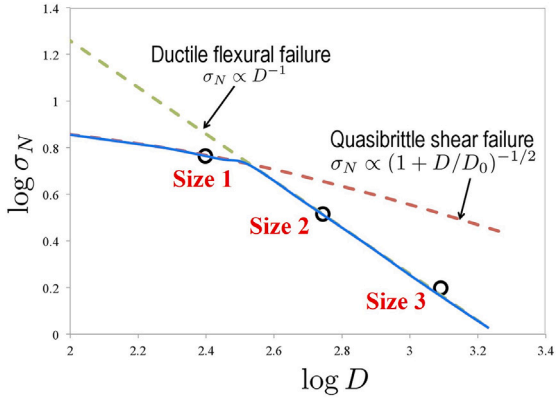

Fig. 29. Numerical simulation of size effect on nominal structural strength [53,65].
Source: Redrawn from [53].

Consequently, only the diagonal shear failure mode would manifest, potentially exhibiting a significant size effect in the absence of shear stirrups.

Even though this research provided relevant basic results on the geometrical effects in HSTCBs with different sizes, further insights would be useful for analysing the influence of the complex geometry of the steel truss on the size effect, and the impact of three-dimensional instead of two-dimensional scaling rules. Moreover, the three specimens considered in this study did not follow geometrical similarity; therefore, existing analytical scaling models were not applicable, and the analytical modelling of this complete size effect was infeasible. Therefore, further robust and efficient computational models appear essential for the design process of HSTCBs across different sizes and geometries.

7. Conclusions

This paper presented a systematic review of the most noteworthy scientific results gathered over the past twenty-five years by researchers in Italy and abroad concerning the mechanical performance of HSTCBs. Outcomes of experimental campaigns and proposals of theoretical formulations have been considered. The topics treated in this review were chosen starting from the careful analysis of an extensive literature database, which was investigated considering the following items: beam typology, structural behaviour, specific insights related to the specialised structural member, and research methodology. Considering the first item, beams with bottom steel plate and concrete base have been analysed, equipped with single planar trusses or double space steel joists. Investigations on ribbed and smooth steel reinforcements have been reported, and the behaviour of the beams in both Phase I and Phase II has been mentioned. With regard to the second item, firstly, the behaviour of weldings and inner connections was treated; secondly, this review reported the main findings dealing with the flexural and shear capacity of beams under ultimate and serviceability limit states in monotonic and cyclic loading conditions. Specific insights have been synthesised regarding the inner connections' stress transfer and shear capacity and the behaviour of beam–column joints endowed with HSTCBs connected to RC columns, hybrid trussed columns or concrete-encased steel columns. In general, the review showed that the classical methods of structural engineering were adopted during years to conduct the research, i.e., extensive experimental tests on structural elements and sub-assemblages, whose resistant mechanisms were interpreted by applying existing analytical formulations given by national and international codes, often followed by the proposal of novel expressions for the assessment of the beam capacity. Simplified and detailed FEM simulations were also developed for validation. The analysis of the main research findings on the aforementioned topics allowed us to outline the comments reported hereafter.

Table R1
Research documents from 1972 to 2015.
Legend: A - Phase I; B - Phase II; C - Steel plate; D - Concrete plate; E - Single planar truss; F - Space/double truss; G - Ribbed steel truss; H - Smooth steel truss; I - Flexural strength; J - Shear strength; K - Push-out response; L - Torsional strength/Buckling; M - Cyclic behaviour; N - Seismic behaviour; O - Deformability at SLS and ULS; P - Long-term behaviour; Q - Welding strength; R - Geometrical effects; S - Beam-to-column joint; T - Inner connections; U - Experimental testing; V - Numerical analysis; W - Analytical modelling.

Authors	keyword code	Authors	keyword code
Leone [1]	W	Badalamenti et al. [25]	B C F G I M T U
Papia [96]	I L U W	Vincenzi and Savoia [11]	A C F L V W
Puhali and Smotlack [17]	B C E F H K T U	Amadio et al. [26]	B C D F G H I J M S T U V W
Giordano and Spadea [97]	I U	Colajanni et al. [27]	B C F G H K T W
Sanpaolesi et al. [99]	M S U	Desiderio et al. [28]	B C F K T V W
Giordano et al. [98]	I U W	Sassone and Casalegno [29]	B C D F G I O P U V W
Sanpaolesi et al. [100]	M S U	Amadio and Sorgon [12]	AB C D F H I J M S U W
VV. AA. [18]	B I J	Trentadue et al. [30]	B F H I L V W
Mele et al. [101]	M S U	Quaranta et al. [31]	B E F H I L O V W
Mele and Sassone [102]	M S U	Scotta and Tesser [32]	B D F H M N S U
Hsu et al. [84]	F G I L M N U W	Colajanni et al. [33]	B C F G M N S U
Di Marco [122]	U	Amadio et al. [34]	B C F J U V W
Sassone and Chiorino [105]	P W	Cancelliere et al. [35]	B C F G I J M T U
Izzo et al. [19]	B G H J	Colajanni et al. [13]	A C G Q S T U W
Tullini et al. [20]	B C F H K Q T U W	Tesser and Scotta [36]	B D F H I J U W
Ju et al. [103]	M S T U	Tullini and Minghini [37]	B C F G H I K Q T U V W
Scotta and Tesser [4]	A B C I J U	Colajanni et al. [38]	B C F G H K T V
Borri and Grazini [104]	N	Colajanni et al. [14]	AB C F G K Q T U W
Badalamenti et al. [5]	A B C F G K T U	Chisari and Amadio [39]	B C F G H J U V W
Badalamenti et al. [6]	A C F G J Q T U V W	Colajanni et al. [40]	B C F G J U V W
Amadio et al. [21]	B S U	Colajanni et al. [41]	B C F G J U W
Vincenzi et al. [7]	A I L R V W	Trentadue et al. [42]	B C F H I O V W
Aiello [22]	B C F G H K T U	Djamaluddin et al. [85]	F H I U
Badalamenti et al. [23]	B C F G I M T U V	Colajanni et al. [43]	B C F G K T V W
La Mendola et al. [8]	A C F G Q T U W	Colajanni et al. [44]	B C F G I M T U V
Scotta and Tesser [9]	A B C I J U	Monti and Petrone [45]	B C D F H J U V W
Amadio et al. [10]	A B C F H I J S U V W	Latour et al. [46]	B C F G H K T W
Amato et al. [24]	B C F G M S U	Colajanni et al. [47]	B C F G J V

Table R2
Research documents from 2016 to 2024.
Legend: A - Phase I; B - Phase II; C - Steel plate; D - Concrete plate; E - Single planar truss; F - Space/double truss; G - Ribbed steel truss; H - Smooth steel truss; I - Flexural strength; J - Shear strength; K - Push-out response; L - Torsional strength/Buckling; M - Cyclic behaviour; N - Seismic behaviour; O - Deformability at SLS and ULS; P - Long-term behaviour; Q - Welding strength; R - Geometrical effects; S - Beam-to-column joint; T - Inner connections; U - Experimental testing; V - Numerical analysis; W - Analytical modelling.

Authors	keyword code	Authors	keyword code
Monaco [48]	B C F G J V W	Amir et al. [88]	F H I O U
Campione et al. [49]	B C F G I J T U V W	Colajanni et al. [68]	B C F G M N S V
Colajanni et al. [50]	B C F G M N S U V W	Deligia et al. [15]	AB C F I W
Colajanni et al. [51]	B C F G J W	Pagnotta et al. [69]	B C F G M N S V
Kareemi et al. [52]	B I J U	Etman et al. [89]	F H J R U W
Zhang et al. [95]	H I J U W	Cao et al. [90]	F H J M N S U W
Ballarini et al. [53]	B C F G I J R V W	Caprili et al. [16]	A G H Q U
Colajanni et al. [54]	B C F G H K T V W	Colajanni et al. [70]	B C F G M N S V
Colajanni et al. [55]	B C F G J U W	Colajanni and Pagnotta [71]	B C F G M N S T V
Djamaluddin et al. [86]	F H I O U	Albright et al. [72]	B C F H M N S U
Colajanni et al. [56]	B C D E F G H J K M T V W	Vigneri et al. [73]	B C E H K Q T U V W
Colajanni et al. [57]	B C F G I J M T U W	Pagnotta et al. [74]	B C F G M N S V
Latour et al. [58]	B C F G H J K T V W	Taher et al. [91]	F H I R V
Monaco et al. [59]	B C F G J W	Colajanni et al. [75]	B C F G M N S V
Deng et al. [94]	E H M N S U	Colajanni et al. [76]	B C F G M N S V
Arafa et al. [87]	F H J V	Pagnotta et al. [77]	B C F G M N S U
Colajanni et al. [60]	B C F G J N V W	Monaco et al. [78]	B C F G M N S V
Monaco et al. [61]	B C F G M N S V	Galik and Calvi [79]	B C F H J V W
Pagnotta et al. [62]	B C F G M N S V	Galik and Calvi [80]	B C F H N S V
Colajanni et al. [63]	B C F G M N S V	Albright et al. [81]	B C F H M N S U
Colajanni et al. [64]	B C F G M N S V	Di Cesare et al. [82]	B C F H M N S U V
Ballarini et al. [65]	B C F G I J R V W	Lofty et al. [92]	F H I R V
Latour et al. [66]	B C F G H J K T V W	Colajanni et al. [83]	B C F G M N S
Frans and Tahya [67]	B C F H I U V	Xue et al. [93]	F H I J R U W

- The Phase II behaviour was much more investigated than the Phase I response due to the need to understand the peculiarities of the stress transfer mechanism between steel parts and concrete block under different conditions, i.e., diverse loading schemes (push-out response, flexural and shear strength, behaviour of joints) and various geometrical layouts of the steel joists. Conversely, the behaviour in Phase I mainly concerned the efficacy of weldings in allowing stress distribution, which was appropriately validated through experimental tests.
- Push-out and shear response in Phase II proved to be highly affected by both the geometrical layout and the steel class of the joist. The experimental tests supported by FEM analyses showed that the stress-transfer mechanism in the push-out specimens and the shear strength mechanism in simply-supported beams did

not follow the typical rules of either RC beams or steel-concrete composite elements. Therefore, numerous analytical formulations were proposed over the years to adequately interpret the resistant mechanism and make the tentative to provide code-compliant expressions useful for the practical design of HSTCBs.

- The behaviour of the beam–column joint was significantly influenced by the degradation phenomena in the panel zone due to the small depth of the beam associated with a large amount of longitudinal reinforcement passing through the joint. Pronounced pinching effects were revealed in almost all specimens tested in the different experimental campaigns, producing limits in the energy dissipation capacity of the structure. This issue emerged as a disadvantage in using such a hybrid joint in seismic areas. Therefore, recent research has tried to address this issue by developing novel strategies by equipping the joint with friction dampers and connecting it by exploiting the bottom steel plate of the HSTCB.
- Open issues still remain on two main topics of interest, i.e., the investigation of the long-term performance of HSTCBs and the analysis of the geometrical and size effects. A very limited number of studies is currently available on these issues, which would need further efforts to be validated and extended. In particular, concerning long-term performance, the effects of different geometrical layouts and steel grades of the joist should be analysed to understand how these parameters could affect the long-term deformation of large-span beams. Concerning geometrical and size effects, further computational models should be developed to consider the case of beams scaled according to geometrical similarity criteria and allow the analytical modelling of the complete size effect on HSTCBs.
- Considering the diffused and increasing adoption of HSTCBs in the structural design of large-span structures and infrastructures, the results of the numerous investigations conducted during the last decades should be finally recalled to develop standardised rules and calculation methods which are not yet implemented in the currently available national and international building codes. Further efforts should be made in order to achieve this goal.

CRediT authorship contribution statement

Alessia Monaco: Writing – review & editing, Writing – original draft, Visualization, Validation, Supervision, Software, Resources, Methodology, Investigation, Formal analysis, Data curation, Conceptualization. **Piero Colajanni:** Writing – review & editing, Conceptualization. **Lidia La Mendola:** Writing – review & editing.

Declaration of competing interest

The authors declare that they have no known competing financial interests or personal relationships that could have appeared to influence the work reported in this paper.

References

[1] Leone S. Procedimenti di calcolo per travi REP (Method of calculus of REP beams). Technical report, Associazione Produttori travi REP (REP Beams Producers Association - Italy); 1972.

[2] CSLLPP Italian standard commission for constructions. Linee guida per l'utilizzo di travi tralicciate in acciaio conglobate nel getto di calcestruzzo collaborante e procedure per il rilascio dell'autorizzazione all'impiego (Guidelines for the utilize of steel trussed beams embedded in collaborating concrete and procedures for the release of the authorization to the usage). 2009.

[3] VV. AA., Guida Tecnico Operativa per il professionista. Progettare con le Travi Prefabbricate Reticolari Miste PREM (Technical Operational Guide for the practitioner. Designing with hybrid steel-trussed concrete beams). Technical report, Milan; 2011.

[4] Scotta R, Tesser L. Preliminary experiences and basic concepts on the structural performance of hybrid trussed beams. In: 4th Spec. conference on the conceptual approach to structural design. 2007.

[5] Badalamenti V, Colajanni P, La Mendola L, Pucinotti R, Scibilia N. Prove di push-out su travi reticolari miste (Push-out tests on Hybrid Steel Trussed Concrete Beams). In: Proceedings of 17th C.T.E congress. 2008, p. 183–92 [in Italian].

[6] Badalamenti V, Colajanni P, La Mendola L, Pucinotti R, Scibilia N. Indagine Sperimentale su Tralicci in Acciaio di Travi Reticolari Miste (Experimental investigation on steel trusses of hybrid trussed beams). In: Proceedings of 17th C.T.E congress. 2008, p. 193–202, [in Italian].

[7] Vincenzi L, Mazzotti C, Savoia M. Stabilità in fase I del traliccio metallico delle travi reticolari miste (Stability in the first phase of the steel truss of composite steel truss and concrete beams). In: Proceedings of 17th C.T.E. congress. 2008, p. 741–50 [in Italian].

[8] La Mendola L, Scibilia N, Colajanni P, Badalamenti V. Indagine sperimentale su nodi di tralicci in acciaio di travi reticolari miste (Experimental investigation on joints of steel trusses of hybrid trussed beams). In: Meccanica dei Materiali e delle Strutture, vol. 1(1). 2009, p. 108–23 [in Italian].

[9] Scotta R, Tesser L. Sperimentazione su travi tralicciate miste REP® – NOR (Experimental tests on composite truss beams REP® – NOR). In: Proceedings of 7th Italian workshop on composite structures. Benevento, Italy: Aesse; 2009, p. 69–76 [in Italian].

[10] Amadio C, Sorgon S, Suraci G. Criteri di verifica per un sistema costituito da elementi tralicciati in acciaio inglobati nel calcestruzzo (Verification criteria of a system constituted by steel trussed elements embedded in the concrete). In: Proceedings of 18th C.T.E congress. 2010 [in Italian].

[11] Vincenzi L, Savoia M. Stabilità di tralicci PREM in prima fase (Stability of PREM-beams in the first phase). In: Proceedings of 18th C.T.E congress. 2010, p. 849–58 [in Italian].

[12] Amadio C, Sorgon S. Comportamento ciclico del nodo trave-colonna per Sistemi Reticolari Misti (Cyclic behaviour of beam-to-column joints in hybrid truss systems). In: Guida Tecnico Operativa per il professionista, Progettare con le Travi Prefabbricate Reticolari Miste, PREM. Italy: Tecniche Nuove; 2011, p. 203–11.

[13] Colajanni P, La Mendola L, Recupero A. Experimental test results vs. analytical prediction of welded joint strength in hybrid steel trussed concrete beams (HSTCBs). Eur J Environ Civ Eng 2013;17(8):742–59.

[14] Colajanni P, La Mendola L, Monaco A. Stress transfer mechanism investigation in hybrid steel trussed-concrete beams by push-out tests. J Constr Steel Res 2014;95:56–70.

[15] Deligia M, Congiu E, Marano G, Briseghella B, Fenu L. Structural optimization of composite steel trussed-concrete beams. Procedia Struct Integr 2021;33:613–22.

[16] Caprili S, Salvatore W, Valentini R. Micro and macro structural investigations on welded joints of composite truss steel concrete beams. Adv Mater Sci Eng 2021;1–13.

[17] Puhali R, Smotlack I. Relazione sulle prove di push-out atte a determinare le leggi di carico-scorrimento delle travi in sistema composto tipo REP (Report on the push-out tests fit for the determination of load–slip laws of REP composite truss beams). Technical report, Science of Constructions Institute ActsUniversity of Trieste; 1980 [in Italian].

[18] VV. AA., Prove a flessione ed a taglio effettuate nell'ambito del Consorzio Produttori Travi Rep nel laboratorio della RDB a Pontenure - 1987 e 1990 (Bending and shear tests executed by the Producers Consortium Rep-beams at the RDB Laboratory in Pontenure - 1987 and 1990). Technical report, CSP-Prefabbricati Industry; 1990.

[19] Izzo L, Minelli F, Plizzari G. Le travi reticolari miste nel cammino verso la normativa (The hybrid trussed beams on the path toward the code). In: Proceedings of 16th C.T.E congress. 2006 [in Italian].

[20] Tullini N, Reato P, Cappellozza M. Indagini sperimentali su travi miste acciaio-calcestruzzo con connessione a traliccio (Experimental investigations on hybrid steel–concrete beams with truss connection). In: Proceedings of 16th C.T.E congress. 2006 [in Italian].

[21] Amadio C, Macorini L, Suraci G. Structural performance of a new hybrid RC-encased steel joist system. In: di Prisco M, editor. Advances in reinforced concrete and precast constructions. Milan: Strarrylink; 2008, p. 19–29.

[22] Aiello MA. Analisi sperimentale della connessione acciaio-calcestruzzo nelle travi reticolari miste (Experimental analysis of steel–concrete connection in hybrid truss beams). In: Proceedings of 7th Italian workshop on composite structures. Benevento, Italy: Aesse; 2009, p. 33–42 [in Italian].

[23] Badalamenti V, La Mendola L, Colajanni P. Analisi teorico-sperimentale del comportamento ciclico di sezioni di estremità di travi prefabbricate reticolari miste (Theoretical-experimental analysis of the ciclic behavior of end-sections of hybrid precast trussed beams). In: Proceedings of 13th ANIDIS congress. 2009, p. 1–10 [in Italian].

[24] Amato G, Badalamenti V, Colajanni P, La Mendola L. Comportamento ciclico delle connessioni tra travi prefabbricate reticolari miste e pilastri in c.a. (Cyclic behavior of the connection between hybrid trussed beams and R.C. columns). In: Proceedings of 18th C.T.E congress. 2010, p. 3–12 [in Italian].

[25] Badalamenti V, La Mendola L, Colajanni P. Seismic behavior of hybrid steel trussed concrete beams.. In: Proceedings of 14th European conference earthquake engineering, Ohrid, Macedonia, paper ID 1527. 2010, p. 1–8.

[26] Amadio C, Macorini L, Sorgon S, Suraci G. A novel hybrid system with rc-encased steel joists. Eur J Environ Civ Eng 2011;15(10):1433–63.

[27] Colajanni P, La Mendola L, Monaco A. Modelli per l'interpretazione dei risultati di prove di push-out su travi reticolari miste (Models for the interpretation of push-out tests results on hybrid trussed beams). In: Proceedings of XIV ANIDIS congress on earthquake engineering. 2011, p. 1–10 [in Italian].

[28] Desiderio G, Latour M, Rizzano G. Modellazione analitica e FEM del meccanismo di trasferimento degli sforzi tra fondello in acciaio e calcestruzzo nelle travi PREM (Analytical and FE modeling of the stress transfer mechanism between the steel plate and the concrete in the PREM beams). In: Proceedings of 14th ANIDIS congress. 2011 [in Italian].

[29] Sassone M, Casalegno C. La viscosità delle Travi Prefabbricate Reticolari Miste (Viscosity of Precast Composite Truss Beams). In: Guida Tecnico Operativa Progettare con le Travi Prefabbricate Reticolari Miste PREM. 2011, p. 219–36, Milan [in Italian].

[30] Trentadue F, Quaranta G, Carlo Marano G, Monti G. Simplified lateral-torsional buckling analysis in special truss-reinforced composite steel-concrete beams. J Struct Eng 2011;137(12):1419–27.

[31] Quaranta G, Petrone F, Marano GC, Trentadue F, Monti G. Structural design of composite concrete-steel beams with spatial truss reinforcement elements, vol. 12, (no. 2):2011, p. 155–78.

[32] Scotta R, Tesser L. Comportamento di nodi trave-pilastro sismo-resistenti in struttura mista di tipo tralicciato soggetti ad azioni cicliche (Experimental behavior of beam-column joints of steel truss and concrete composite structure subjected to cyclic loads). In: Progettazione sismica, vol. 3, Italia; 2011, p. 47–62.

[33] Colajanni P, La Mendola L, Monaco A. Analisi sperimentale del comportamento ciclico di nodi di travi SER e pilastri in c.a. (Experimental analysis of the cyclic behavior of SER beam-to-R.C. column joints). In: Proceedings of 19th C.T.E congress. 2012, p. 171–80 [in Italian].

[34] Amadio C, Chisari C, Plizzari G, Minelli F. Indagini preliminari sul comportamento a taglio delle travi PREM (Preliminary Investigations on the shear behavior of PREM beams). In: Proceedings of 19th C.T.E congress. 2012, p. 101–12 [in Italian].

[35] Cancelliere N, Colajanni P, La Mendola L. On bottom steel plate to concrete anchorage in hybrid steel trussed concrete beams. In: Proceedings of STESSA 2012 - behaviour of steel structures in seismic areas. London: CRC Press/Balkema Publishers – Taylor and Francis Group; 2012, p. 243–8, 2011.

[36] Tesser L, Scotta R. Flexural and shear capacity of composite steel truss and concrete beams with inferior precast concrete base. Eng Struct 2013;49:135–45.

[37] Tullini N, Minghini F. Nonlinear analysis of composite beams with concrete-encased steel truss. J Constr Steel Res 2013;91:1–13.

[38] Colajanni P, La Mendola L, Monaco A, Latour M, Rizzano G. Assessment of push-out test response of hybrid steel trussed-concrete beams by FE model. In: Proceedings of XV ANIDIS congress on earthquake engineering. 2013, p. 1–10.

[39] Chisari C, Amadio C. An experimental, numerical and analytical study of hybrid RC-encased steel joist beams subjected to shear. Eng Struct 2014;61:84–98.

[40] Colajanni P, La Mendola L, Mancini G, Recupero A, Spinella N. Shear capacity in concrete beams reinforced by stirrups with two different inclinations. Eng Struct 2014;81(1):444–53.

[41] Colajanni P, La Mendola L, Monaco A. Analisi teorico-sperimentale del comportamento a taglio di travi prefabbricate reticolari miste (Experimental and theoretical analysis of the shear behavior of hybrid steel trussed-concrete beams). In: Proceedings of 20th C.T.E congress. 2014, p. 151–61 [in Italian].

[42] Trentadue F, Mastromarino E, Quaranta G, Petrone F, Monti G, Marano GC. Bending stiffness of truss-reinforced steel-concrete composite beams. Open J Civ Eng 2014;4:285–300.

[43] Colajanni P, La Mendola L, Latour M, Monaco A, Rizzano G. FEM analysis of push-out test response of hybrid steel trussed concrete beams (HSTCBs). J Constr Steel Res 2015;111:88–102.

[44] Colajanni P, La Mendola L, Monaco A. Stiffness and strength of composite truss beam to R.C. column connection in MRFs. J Constr Steel Res 2015;113:86–100.

[45] Monti G, Petrone F. Shear resisting mechanisms and capacity equations for composite truss beams. J Struct Eng (United States) 2015;141(12).

[46] Latour M, Monaco A, Rizzano G. Evaluation of the shear connection strength of precast hybrid steel-trussed-concrete composite beams. In: Proceedings of XXV CTA congress (XXV Italian steel days), vol. 1. 2015, p. 271–84.

[47] Colajanni P, La Mendola L, Monaco A. Finite element modeling of the shear behavior of hybrid steel trussed concrete beams. In: Proceedings of XXV CTA congress (XXV Italian steel days), vol. 1,. 2015, p. 261–70.

[48] Monaco A. Numerical prediction of the shear response of semi-prefabricated steel-concrete trussed beams. Constr Build Mater 2016;124:462–74.

[49] Campione G, Colajanni P, Monaco A. Analytical evaluation of steel–concrete composite trussed beam shear capacity. Mater Struct/Mater Constr 2016;49(8):3159–76.

[50] Colajanni P, La Mendola L, Monaco A, Spinella N. Cyclic behavior of composite truss beam-to-RC column joints in MRFS. Key Eng Mater 2016;711:681–9.

[51] Colajanni P, La Mendola L, Monaco A, Recupero A. Validation of a shear model for RC and hybrid beams with two different inclinations of transversal reinforcement. In: Advances in civil and infrastructure engineering II. Applied mechanics and materials, vol. 847, Trans Tech Publications Ltd; 2016, p. 505–12.

[52] Kareemi MA, Petrone F, Monti G. Experimental tests on composite steel-concrete truss beams. In: Advances in civil and infrastructure engineering II. Applied mechanics and materials, vol. 847, Trans Tech Publications Ltd; 2016, p. 68–75.

[53] Ballarini R, La Mendola L, Le J-L, Monaco A. Computational study of failure of hybrid steel trussed concrete beams. J Struct Eng (United States) 2017;143(8).

[54] Colajanni P, La Mendola L, Latour M, Monaco A, Rizzano G. Analytical prediction of the shear connection capacity in composite steel–concrete trussed beams. Mater Struct/Mater Constr 2017;50(1).

[55] Colajanni P, La Mendola L, Monaco A. Experimental investigation of the shear response of precast steel-concrete trussed beams. J Struct Eng (United States) 2017;143(1).

[56] Colajanni P, La Mendola L, Monaco A. Review of push-out and shear response of hybrid steel-trussed concrete beams. Buildings 2018;8(10).

[57] Colajanni P, La Mendola L, Monaco A. Stress transfer and failure mechanisms in steel-concrete trussed beams: Experimental investigation on slab-thick and full-thick beams. Constr Build Mater 2018;161:267–81.

[58] Latour M, Monaco A, Rizzano G. Modeling of the shear connection capacity of hybrid steel trussed composite beams. In: Proceedings of Italian concrete days. 2018, p. 1–10.

[59] Monaco A, Colajanni P, La Mendola L. Comparative analysis of shear resisting models for hybrid steel trussed concrete beams. In: Proceedings of Italian concrete days. 2018, p. 1–10 [in Italian].

[60] Colajanni P, Mendola L, Monaco A. Shear models of Rc-encased steel joist beams in MRFs. Ingegneria Sismica 2019;36(2):14–30.

[61] Monaco A, Pagnotta S, Colajanni P, La Mendola L. Dissipative connections of RC frames with prefabricated steel-trussed-concrete beams. In: Proceedings of XXVII CTA congress (XXVII Italian steel days). 2019, p. 379–88.

[62] Pagnotta S, Colajanni P, La Mendola L, Monaco A. Seismic response of RC frames with HSTC beams endowed with friction damper devices. In: Proceedings of XVIII ANIDIS congress on earthquake engineering. 2019, p. 2942–52.

[63] Colajanni P, La Mendola L, Monaco A, Pagnotta S. Design of friction connections in RC structures with hybrid steel-trussed-concrete beams. In: Proceedings of XVIII ANIDIS congress on earthquake engineering. 2019, p. 2960–8.

[64] Colajanni P, La Mendola L, Monaco A, Pagnotta S. Dissipative connections of RC frames with prefabricated steel-trussed-concrete beams. Ingegneria Sismica 2020;37(1):51–63.

[65] Ballarini R, Mendola L, Le J, Monaco A. Computational assessment of the structural performance of concrete beams with encased steel joist. In: Proceedings of the 6th European conference on computational mechanics ECCM 2018. 2020, p. 1187–98.

[66] Latour M, Monaco A, Rizzano G. Modeling of the shear connection capacity of hybrid steel trussed composite beams. Lect Notes Civ Eng 2020;42:149–61.

[67] Frans PL, Tahya H. Behavior of concrete beam deflection framework system. In: Proceeding on international conference of science management art research technology. 2020.

[68] Colajanni P, La Mendola L, Monaco A, Pagnotta S. Design of RC joints equipped with hybrid trussed beams and friction dampers. Eng Struct 2021;227.

[69] Pagnotta S, Monaco A, Colajanni P, La Mendola L. Beam-to-column friction connection for earthquake-resilient reinforced concrete frames made with hybrid trussed beams. In: Proceedings of 2nd fib symposium on concrete and concrete structures. 2021, p. 1–10.

[70] Colajanni P, La Mendola L, Monaco A, Pagnotta S. Seismic performance of earthquake-resilient RC frames made with HSTC beams and friction damper devices. J Earthq Eng 2022;26(15):7787–813.

[71] Colajanni P, Pagnotta S. Friction-based beam-to-column connection for low-damage RC frames with hybrid trussed beams. Steel Compos Struct 2022;45(2):231–48.

[72] Albright A, Argentoni A, Calvi P. Experimental behavior of interior and exterior steel-concrete composite NPS® beam-column joints. Eng Struct 2022;251.

[73] Vigneri V, Kroyer R, Taras A. Experimental study on the longitudinal shear transfer mechanisms and resistance in CSTC composite beams. Structures 2022;45:2022–37.

[74] Pagnotta S, Monaco A, M A, Colajanni P, La Mendola L. Replaceable friction device for steel-concrete composite trussed beam-to-RC column joint. In: Proceedings of XXVIII CTA congress (XXVIII Italian steel days). 2022, p. 879–87.

[75] Colajanni P, La Mendola L, Monaco A, Pagnotta S. Low-damage friction connections in hybrid joints of frames of reinforced-concrete buildings. Appl Sci (Switzerland) 2023;13(13).

[76] Colajanni P, La Mendola L, Monaco A, Pagnotta S. Seismic response of RC frames with steel-concrete truss beams equipped with beam-to-column and column-to-foundation friction damper connections. Lect Notes Civ Eng 2023;351:605–21.

[77] Pagnotta S, Monaco A, Colajanni P, La Mendola L. Experimental characterization of friction properties of materials for innovative beam-to-column dissipative connection for low-damage RC structures. Procedia Struct Integr 2023;44:1909–16.

[78] Monaco A, Pagnotta S, Colajanni P, La Mendola L. Innovative connections for steel-concrete-trussed beams: a patented solution. Procedia Struct Integr 2023;44:1925–32.
[79] Galik W, Calvi P. Shear strength of steel-concrete composite "NPS® Basic" truss beams. Eng Struct 2023;290.
[80] Galik W, Calvi P. Numerical modeling of a novel steel-concrete composite beam-column joint solution. In: COMPDYN proceedings. 2023.
[81] Albright JA, Argentoni A, Calvi PM. Experimental investigation of interior and exterior steel-concrete composite NPS® beam-column joints. In: Ce/papers - proceedings in civil engineering 6(1). 2023, p. 599–610.
[82] Di Cesare A, Belviso P, Ponzo FC, Vitone G. Seismic behavior and modeling of ductile composite steel-trussed concrete beam to column joints. Appl Sci (Switzerland) 2023;13(20).
[83] Colajanni P, Ahmed M, Pagnotta S, Orlando P. A review of friction dissipative beam-to-column connections for the seismic design of MRFs. Appl Sci 2024;14(6).
[84] Hsu H-L, Hsieh J-C, Juang J-L. Seismic performance of steel-encased composite members with strengthening cross-inclined bars. J Constr Steel Res 2004;60(11):1663–79.
[85] Djamaluddin RDR, Bachtiar Y, Irmawati R, Akkas AM, Latief RU. Effect of the truss system to the flexural behavior of the external reinforced concrete beams. J Civ Environ Eng 2014;8:691–5.
[86] Djamaluddin RDR, Frans PL, Irmawati R. Flexural capacity of the concrete beams reinforced by steel truss system. In: MATEC web conference - the 6th international conference of Euro Asia civil engineering forum. 2017.
[87] Arafa M, Alqedra MA, Salim R. Performance of RC beams with embedded steel trusses using nonlinear FEM analysis. Adv Civ Eng 2018;2018.
[88] Amir A, Djamaluddin RDR, Irmawaty R, Amiruddin A, Fakhruddin. Failure mode of truss system concrete beams strengthened with tensile reinforcement. In: IOP conference series: Earth and environmental science, vol. 419, 2020.
[89] Etman EE, Afefy HM, Baraghith AT, Abuelwafa M. Shear behavior of RC beams reinforced with internal trussed steel strips at shear span zone. Structures 2021;32:1734–51.
[90] Cao D, Liu J, Ge W, Qian R. Experimental study on the shear performance of steel-truss-reinforced concrete beam-column joints. Adv Civ Eng 2021;2021.
[91] Taher SE-DF, Afefy HM, Fawzy O, Salem S. Numerical simulation of RC beams reinforced with internal steel trusses. Int J Adv Struct Geotech Eng 2022.
[92] Lofty E, Kamal I, Hassan M, Hassan K. Flexural investigation of a composite trussed-beam for aerospace shelters using numerical modelling. Journal of Physics: Conference Series 2023;2616(1).
[93] Xue H, Ashour A, Ge W, Cao D, Sun C, Liu J. Experimental study on mechanical behavior of steel truss-reinforced concrete box girders. J Constr Steel Res 2024;212.
[94] Deng Z, Hu Q, Zeng J, Xiang P, Xu C. Structural performance of steel-trussreinforced composite joints under cyclic loading. Proc Inst Civ Eng Struct Build 2018;171(2):130–48.
[95] Zhang N, Fu CC, Chen L, He L. Experimental studies of reinforced concrete beams using embedded steel trusses. ACI Struct J 2016;113(4):701–10.
[96] Papia M. Indagine teorica e sperimentale sui fenomeni di instabilità flesso-torsionale nelle travi REP (Theoretical and experimental investigation on the flexural-torsional buckling phenomena of the REP beams). Technical report, Italy: Science of Constructions Institute Acts, University of Palermo; 1977.
[97] Giordano G, Spadea G. Stato Ultimo in flessione di travi in cemento armato con doppia armatura tipo REP: ricerca sperimentale (Flexural ultimate state of reinforced concrete beams with double reinforcement REP type: experimental research). Report no. 65. Technical report, Italy: Structural Department of University of Calabria; 1983.
[98] Giordano G, Ombres L, Spadea G. Modellazione teorica e controllo sperimentale del comportamento a rottura di travi inflesse di tipo REP (Theoretical modelling and experimental verification of the collapse behaviour of REP type bended beams). In: L'industria Italiana del cemento. 1987, p. 617.
[99] Sanpaolesi L, Caramelli S, Croci P. Indagine sperimentale su nodi di elementi prefabbricati trave- pilastro sotto fatica in campo plastico. (Experimental investigation on beam-to-column precast joints under fatigue in the plastic field). In: Proceedings of AICAP. 1987, p. 543–57 [in Italian].
[100] Sanpaolesi L, Croci P, Viviani M. Influenza del confinamento del calcestruzzo sul comportamento a fatica oligociclica di nodi trave – pilastro prefabbricati: indagine sperimentale (Concrete confinement influence on the oligocyclic fatigue behavior of precast beam-to-column joints: experimental investigation). In: Proceedings of 7th C.T.E congress. 1988, p. 63–70, (in Italian).
[101] Mele M, Ciampoli M, Menegatti E. Nuovi sistemi strutturali composti di acciaio e calcestruzzo: prime analisi sperimentali del comportamento sotto azioni cicliche dei nodi travi - pilastro (New structural steel-concrete composite systems: first experimental analyses of beam-to-column joints under cyclic actions). In: Proceedings of 1st Italian workshop on composite structures. 1993, p. 85–98 [in Italian].
[102] Mele M, Sassone M. Sistemi strutturali composti ad armatura superficiale: indagine sperimentale sul comportamento di nodi travi - pilastro soggetti a carichi ciclici. (Composite structural systems with superficial reinforcement: experimental investigation on the behavior under cyclic loads of beam-to-column joints). In: Proceedings of 5th Italian workshop on composite structures. 2002, p. 191–200 [in Italian].
[103] Ju YK, Kim J-Y, Kim S-D. Experimental evaluation of new concrete encased steel composite beam to steel column joint. J Struct Eng 2007;133(4):519–29.
[104] Borri A, Grazini A. Analisi del comportamento di travi tralicciate in c.a. per il miglioramento della risposta sismica degli edifici (Analysis of the reinforced concrete truss beam behaviour for the improvement of the building seismic capacity). In: Proceedings of XII ANIDIS congress on earthquake engineering. 2007.
[105] Sassone M, Chiorino M. Design aids for the evaluation of creep induced structural effects. American Concrete Institute, ACI Special Publication; 2005, p. 239–60, SP-227.
[106] van Eck NJ, Waltman L. Manual for VOSviewer version 1.6.20. Univ Leiden 2023;1:1–55.
[107] EN 1994-1-1:2004 Eurocode 4: Design of composite steel and concrete structures – Part 1-1: General rules and rules for buildings. In: Eurocode 4, Brussels, Belgium: European Committee for Standardization (CEN); 2004.
[108] EN1993-1-1:2005 Eurocode 3: Design of steel structures - part 1-1: General rules and rules for buildings. In: Eurocode 3, Brussels, Belgium: European Committee for Standardization (CEN); 2005.
[109] Vintzēleou EN, Tassios TP. Eccentric dowels loaded against core of concrete sections. J Struct Eng 1990;116(10):2621–33.
[110] Millard SG, Johnson RP. Shear transfer across cracks in reinforced concrete due to aggregate interlock and to dowel action. Mag Concr Res 1984;36(126):9–21.
[111] EN1992-1-1:2004 eurocode 2: Design of concrete structures - part 1-1: General rules and rules for buildings. In: Eurocode 2, Brussels, Belgium: European Committee for Standardization (CEN); 2004.
[112] fib Bulletin No. 56: Model code 2010 - First complete draft, vol. 2. Lausanne, Switzerland: Fédération Internationale du Béton (fib); 2010.
[113] Hwang S-J, Lee H-J. Strength prediction for discontinuity regions by softened strut-and-tie model. J Struct Eng 2002;128(12):1519–26.
[114] Kim J, LaFave J, Song J. Joint shear behaviour of reinforced concrete beam–column connections. Mag Concr Res 2009;61(2):119–32.
[115] Colajanni P, La Mendola L, Monaco A, Pagnotta S, (Inventors). Seismic dissipation system for building structures. Patent n. 102019000016742. 2019.
[116] Bažant ZP. Size effect in blunt fracture: Concrete, rock, metal. J Eng Mech 1984;110(4):518–35.
[117] Carpinteri A. Scaling laws and renormalization groups for strength and toughness of disordered materials. Int J Solids Struct 1994;31(3):291–302.
[118] Carpinteri A. Cusp catastrophe interpretation of fracture instability. J Mech Phys Solids 1989;37(5):567–82.
[119] Bosco C, Carpinteri A, Debernardi P. Fracture of reinforced concrete: Scale effects and snap-back instability. Eng Fract Mech 1990;35(4–5):665–77.
[120] Carpinteri A, Accornero F. Dimensional analysis of critical phenomena: Self-weight failure, turbulence, resonance, fracture. Phys Mesomech 2021;24(4):459–63.
[121] Bažant ZP. Scaling of structural strength. 2nd ed. London: Hermes-Penton Science; 2005.
[122] Di Marco R. Sperimentazione su travi continue REP con traliccio tipo TR (Experimental tests on hyperstatic REP beams with TR truss type). Technical report, Italy: Internal Report University IUAV of Venice; 2004.